Supporting information

Towards Rational Design of TADF Two-coordinate Coinage Metal Complexes: Understanding the Relationship between Natural Transition Orbital Overlap and Photophysical Properties

Tian-yi Li[a,b], Jonas Schaab[a], Peter I. Djurovich[a], Mark E. Thompson[a*]

[a] Department of Chemistry, University of Southern California, Los Angeles, CA, USA

[b] School of Chemistry and Biological Engineering, Department of Physical Chemistry, University of Science and Technology Beijing, Beijing, 100083, China

Email: met@usc.edu

Contents

General information

All reactions were carried out using Schleck line system under N_2 in oven dried glassware. Organic and inorganic materials were used as commercial grade without further purifications. Anhydrous solvents were purified by Class Contour solvent system by SG Water USA, LLC. ^{1}H and ^{13}C NMR spectra were recorded on a Varian Mercury 400 instrument. Elemental analyses were performed at University of Southern California, using a Fisher CHNS 2000 instrument.

Syntheses and characterization

General procedure for the carbene precursors

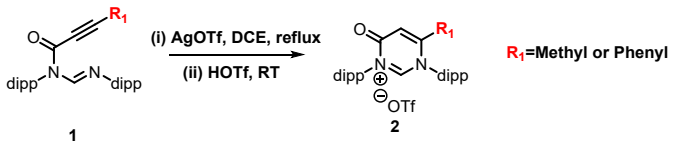

The methyl or phenyl substituted acetylenyl formamidine **1** was synthesized according to previous method, and the following 6-endo-dig cyclization was performed using a modified procedure.[1, 2] Equal equivalent of **1** (500 mg) and AgOTf (300 mg) were dissolved in 20 mL dichloromethane (DCE) in a sealed glass vial. The solution was refluxed for 1h and the clear colorless solution turned into dark brown suspension with Ag mirror on the wall. After cooling down to room temperature, the suspension was filtrated through Celite. The filtration was injected to another sealed vial and 1 equiv. of HOTf was added dropwise. The system was stirred at room temperature for another 1h. The solution was filtered through Celite. After removing all the volatiles, the raw product was washed by cold ether for three times, giving the carbene precursors as white powder.

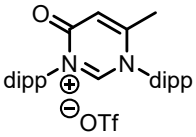

Obtained 300 mg, yield 91%. ^{1}H NMR (400 MHz, acetone) δ 10.35 (s, 1H), 7.80 – 7.74 (m, 1H), 7.69 – 7.60 (m, 3H), 7.52 (d, J = 7.8 Hz, 2H), 7.36 (s, 1H), 2.99 (sept, J = 6.7 Hz, 2H), 2.89 (sept, J = 6.8 Hz, 2H), 2.33 (d, J = 1.1 Hz, 3H), 1.38 (d, J = 6.7 Hz, 6H), 1.28 (d, J = 6.8 Hz, 12H), 1.19 (d, J = 6.7 Hz, 6H).

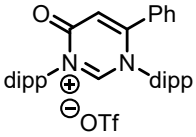

Obtained 298 mg, yield 93%. ^{1}H NMR (400 MHz, acetone) δ 10.41 (d, J = 0.5 Hz, 1H), 7.70 – 7.64 (m, 1H), 7.62 – 7.55 (m, 1H), 7.55 – 7.50 (m, 3H), 7.47 (t, J = 1.4 Hz, 1H), 7.46 – 7.38 (m, 6H), 3.20 (sept, J = 6.7 Hz, 2H), 2.98 (sept, J = 6.7 Hz, 2H), 1.30 (d, J = 6.8 Hz, 6H), 1.24 (d, J = 6.8 Hz, 6H), 1.19 (d, J = 6.7 Hz, 6H), 1.16 (d, J = 6.6 Hz, 6H).

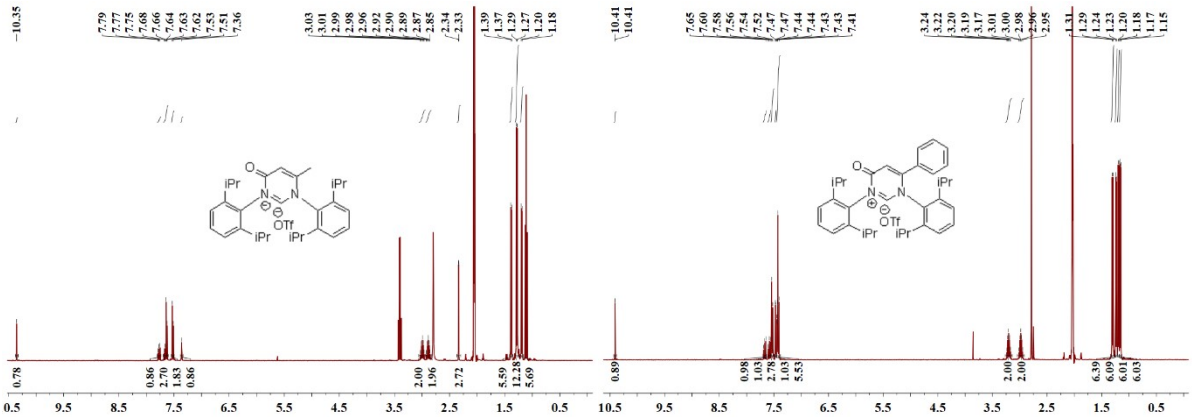

Figure S1 ^{1}H NMR spectra of the carbene precursors

Synthesis of the Cu complexes

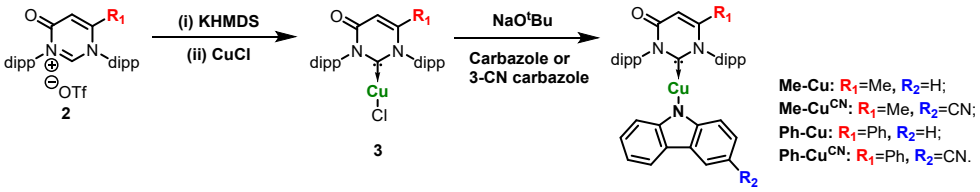

Carbene precursor was dissolved in 150 mL anhydrous THF at room temperature and 1.05 euqiv. of KHMDS (0.5M in toluene) was injected dropwise. After stirring at room temperature for 3h, 1.1 euqiv. of CuCl was added in one portion and the system was kept stirring for overnight. Then, the mixture was filtered through Celite. After removing the volatiles, the residue was sonicated in ether giving the intermediate complex **3** as beige powder (yield around 60%), which was used in the following reactions without further purifications.

Me-Cu, **Me-Cu^{CN}**, **Ph-Cu** and **Ph-Cu^{CN}** were synthesized according to a known procedure which was well described in previous publications.[3-5]

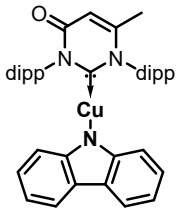

Me-Cu was obtained with a yield of 80% as yellow powder. ^{1}H NMR (400 MHz, acetone) δ 7.93 (t, J = 7.8 Hz, 1H), 7.81 (t, J = 7.8 Hz, 1H), 7.74 (d, J = 7.6 Hz, 2H), 7.69 (d, J = 7.9 Hz, 2H), 7.58 (d, J = 7.8 Hz, 2H), 6.85 (ddd, J = 8.2, 7.0, 1.3 Hz, 2H), 6.79 – 6.69 (m, 3H), 5.60 (d, J = 8.1 Hz, 2H), 2.99 (sept, J = 6.7 Hz, 4H), 2.15 (d, J = 0.9 Hz, 3H), 1.39 (d, J = 6.8 Hz, 6H), 1.28 (d, J = 6.8 Hz, 6H), 1.23 (dd, J = 9.5, 6.9 Hz, 12H). ^{13}C NMR (101 MHz, acetone) δ 158.51, 155.04, 149.80, 145.77, 145.62, 136.99, 135.97, 131.48, 130.39, 125.86, 124.91, 123.95, 122.78, 118.44, 115.09, 114.58, 111.72, 29.65, 28.75, 28.33, 24.72, 23.63, 23.37, 22.60, 20.18. Elemental analysis calculated C 74.57, H 7.02, N 6.36; found C 74.24, H ,7.05 N 6.13.

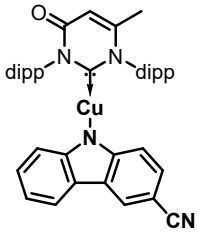

Me-Cu^{CN} was obtained with a yield of 77% as bright yellow powder. ^{1}H NMR (400 MHz, acetone) δ 8.18 – 8.12 (m, 1H), 7.97 (t, J = 7.8 Hz, 1H), 7.90 – 7.81 (m, 2H), 7.71 (d, J = 7.9 Hz, 2H), 7.59 (d, J = 7.8 Hz, 2H), 7.11 (dd, J = 8.5, 1.7 Hz, 1H), 6.98 (ddd, J = 8.2, 7.1, 1.3 Hz, 1H), 6.88 (td, J = 7.5, 1.0 Hz, 1H), 6.74 (d, J = 1.0 Hz, 1H), 5.65 (d, J = 8.1 Hz, 1H), 5.55 (dd, J = 8.5, 0.5 Hz, 1H), 3.06 – 2.91 (m, 4H), 2.15 (s, 3H), 1.38 (d, J = 6.8 Hz, 6H), 1.24 (dd, J = 10.7, 6.8 Hz, 12H), 1.19 (d, J = 6.9 Hz, 6H). ^{13}C NMR (101 MHz, acetone) δ 158.41, 155.07, 151.55, 150.44, 145.87, 145.70, 136.99, 135.98, 131.67, 130.59, 125.98, 125.66, 125.02, 124.52, 124.19, 123.75, 123.23, 121.35, 119.26, 117.12, 115.12, 115.05, 112.01, 96.85, 28.86, 24.76, 23.64, 23.37, 22.57, 20.17. Elemental analysis calculated C 73.60, H 6.62, N 8.17; found C 73.08, H 6.44, N 7.99.

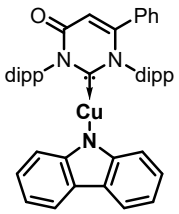

Ph-Cu was obtained with a yield of 82% as yellow powder. ^{1}H NMR (400 MHz, acetone) δ 7.82 (t, J = 7.8 Hz, 1H), 7.77 – 7.70 (m, 3H), 7.60 (d, J = 7.8 Hz, 2H), 7.47 (d, J = 7.9 Hz, 3H), 7.37 (dd, J = 5.1, 1.5 Hz, 4H), 6.82 (ddd, J = 8.2, 7.0, 1.3 Hz, 2H), 6.78 (s, 1H), 6.71 (td, J = 7.4, 1.0 Hz, 2H), 5.59 – 5.53 (m, 2H), 3.12 (dhept, J = 20.3, 6.6 Hz, 4H), 1.29 (d, J = 6.8 Hz, 6H), 1.26 (d, J = 6.8 Hz, 6H), 1.23 (d, J = 6.9 Hz, 6H), 1.17 (d, J = 6.7 Hz, 6H). ^{13}C NMR (101 MHz, acetone) δ 158.40, 156.70, 149.77, 146.05, 145.93, 137.53, 136.00, 131.73, 131.34, 130.59, 130.50, 129.35, 128.21, 125.44, 125.03, 123.96, 122.75, 118.42, 115.06, 114.62, 113.14, 28.85, 25.51, 23.68, 23.63, 21.96. Elemental analysis calculated C 76.48, H 6.70, N 5.82; found C 76.23, H 6.44, N 5.64.

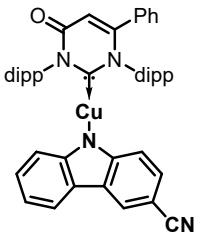

Ph-Cu^{CN} was obtained with a yield of 75% as bright yellow powder. ^{1}H NMR (400 MHz, acetone) δ 8.16 (s, 1H), 7.89 (t, *J* = 7.9 Hz, 2H), 7.81 (t, *J* = 7.8 Hz, 1H), 7.64 (d, *J* = 7.8 Hz, 2H), 7.51 (t, *J* = 6.6 Hz, 2H), 7.49 – 7.44 (m, 1H), 7.40 (dd, *J* = 8.7, 5.3 Hz, 4H), 7.11 (dd, *J* = 8.5, 1.5 Hz, 1H), 6.98 (t, *J* = 7.1 Hz, 1H), 6.89 (t, *J* = 7.3 Hz, 1H), 6.83 (s, 1H), 5.65 (d, *J* = 8.1 Hz, 1H), 5.54 (d, *J* = 8.5 Hz, 1H), 3.15 (dtd, *J* = 20.4, 13.5, 6.7 Hz, 4H), 1.29 (t, *J* = 7.3 Hz, 12H), 1.24 (d, *J* = 6.8 Hz, 6H), 1.19 (d, *J* = 6.7 Hz, 6H). ^{13}C NMR (101 MHz, acetone) δ 158.31, 156.66, 151.51, 150.42, 146.12, 146.03, 137.58, 136.02, 131.61, 131.52, 130.70, 130.67, 129.34, 128.25, 125.63, 125.56, 125.15, 124.49, 124.20, 123.72, 123.24, 121.35, 119.24, 117.09, 115.16, 115.10, 113.41, 96.81, 28.84, 25.57, 23.69, 23.64, 21.93. Elemental analysis calculated C 75.52, H 6.34, N 7.50; found C 75.38, H 6.07, N 7.27.

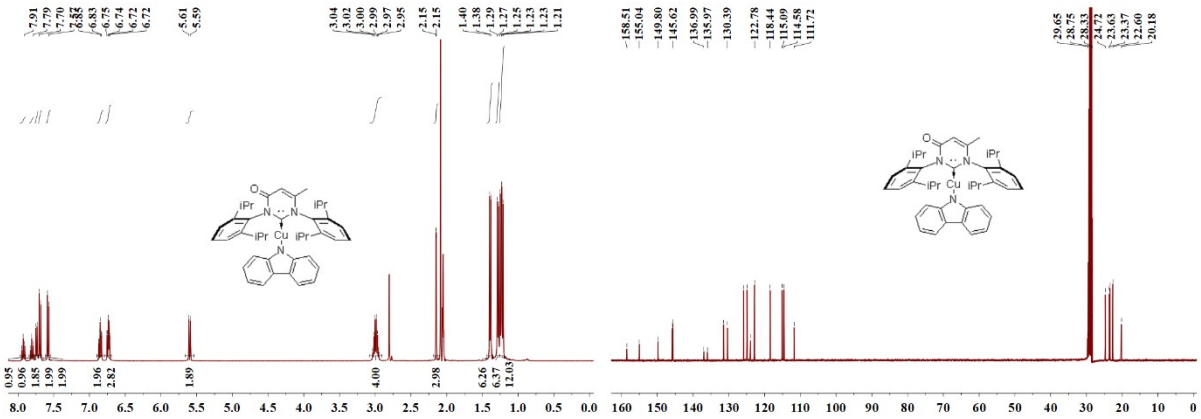

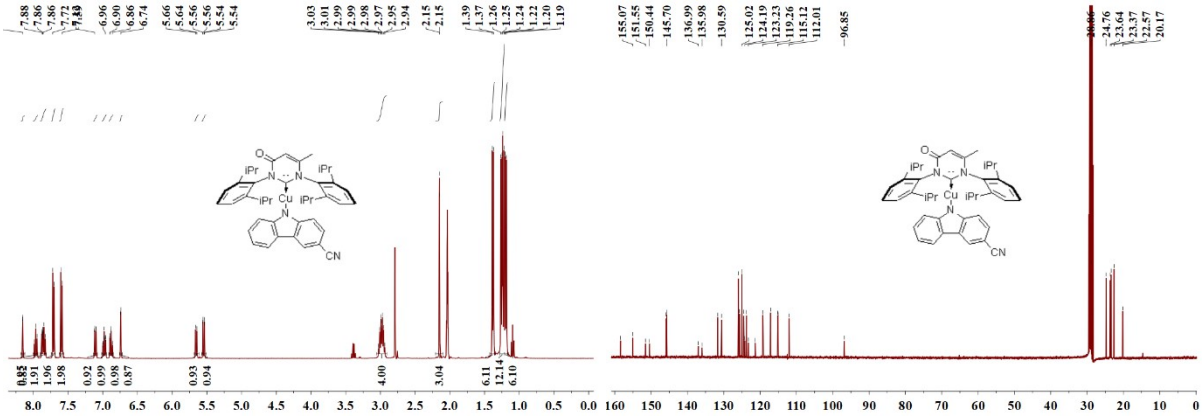

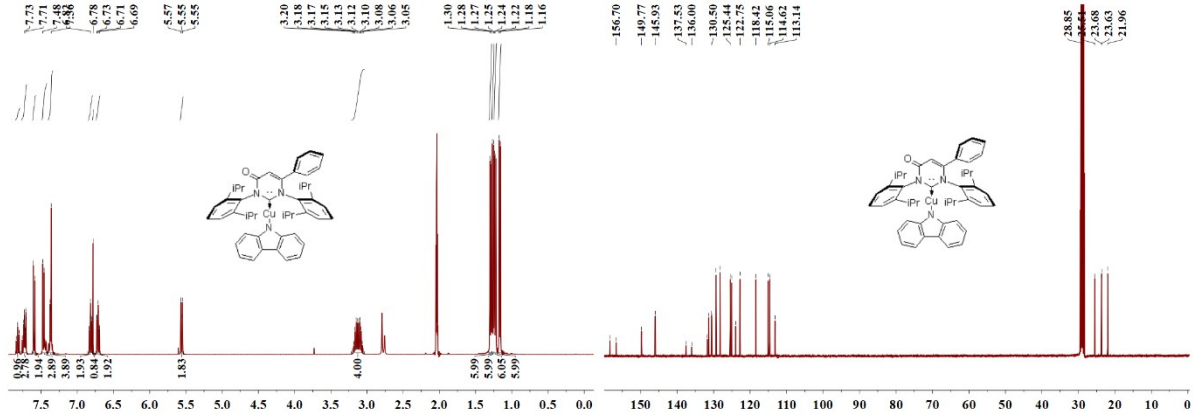

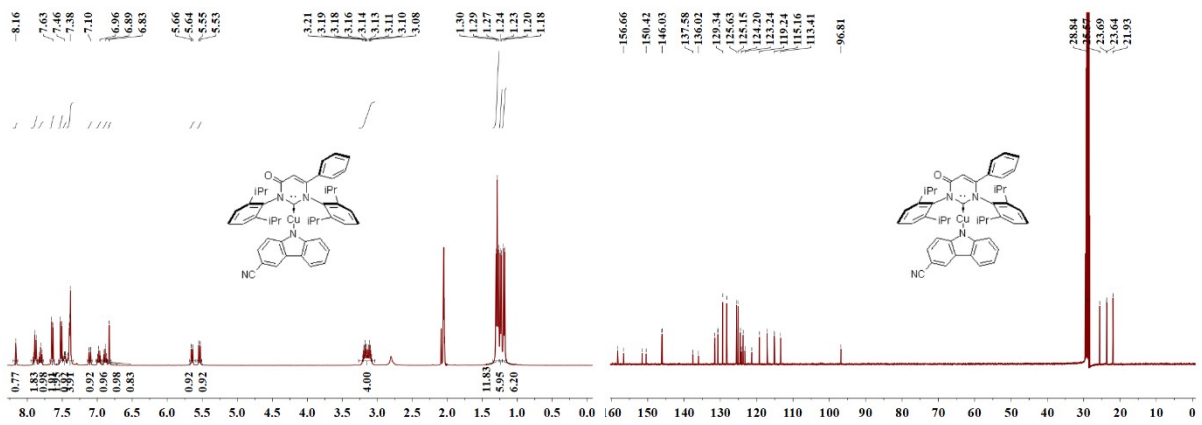

Figure S2 ^{1}H NMR and ^{13}C NMR spectra of the Cu(I) complexes

Synthesis of the Ag complexes

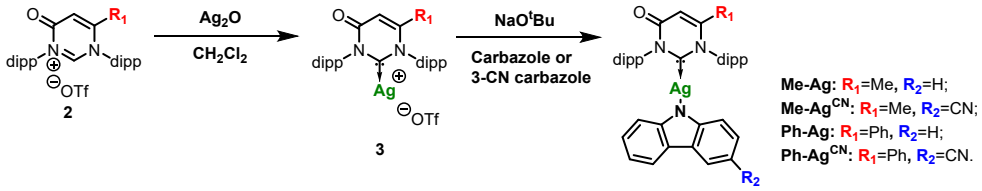

Carbene precursor and 0.7 euqiv. of Ag_2O were stirred in 50 mL anhydrous CH_2Cl_2 at room temperature for 48h with a coverage of aluminum foil. After removing the insoluble precipitates by filtration through Celite, the filtrate was dried to afford raw product. Then, the oily raw product was sonicated in ether to provide the final product as light purple powder (yield over 90%), which was used in the following reactions without further purifications.

Me-Ag, **Me-Ag^{CN}**, **Ph-Ag** and **Ph-Ag^{CN}** were synthesized according to a known procedure which was well described in previous publications.[3-5]

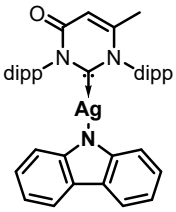

Me-Ag was obtained with a yield of 79% as orange powder. ^{1}H NMR (400 MHz, acetone) δ 7.88 (t, J = 7.7 Hz, 1H), 7.77 (t, J = 9.2 Hz, 3H), 7.68 (d, J = 7.8 Hz, 2H), 7.56 (d, J = 7.8 Hz, 2H), 6.93 (ddd, J = 8.1, 7.0, 1.2 Hz, 2H), 6.80 – 6.70 (m, 3H), 6.04 (d, J = 8.1 Hz, 2H), 2.98 (dq, J = 13.4, 6.6 Hz, 4H), 2.23 (s, 3H), 1.39 (d, J = 6.8 Hz, 6H), 1.34 (d, J = 6.8 Hz, 6H), 1.28 (d, J = 6.9 Hz, 6H), 1.24 (d, J = 6.8 Hz, 6H). ^{13}C NMR (101 MHz, acetone) δ 158.35, 158.30, 154.91, 154.84, 150.29, 145.41, 145.28, 138.25, 137.47, 131.43, 130.36, 125.81, 124.81, 123.84, 122.79, 118.59, 114.58, 114.44, 112.21, 28.84, 28.66, 24.71, 23.63, 23.50, 22.86, 20.49, 20.48. Elemental analysis calculated C 69.88, H 6.58, N 5.96; found C 69.43, H 6.52, N 5.86.

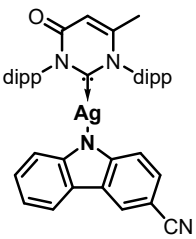

Me-Ag^{CN} was obtained with a yield of 75% as yellow powder. ^{1}H NMR (400 MHz, acetone) δ 8.21 (s, 1H), 7.94 (t, J = 7.9 Hz, 2H), 7.82 (t, J = 7.8 Hz, 1H), 7.71 (d, J = 7.8 Hz, 2H), 7.60 (d, J = 7.8 Hz, 2H), 7.21 (dd, J = 8.5, 1.6 Hz, 1H), 7.08 (t, J = 7.6 Hz, 1H), 6.91 (t, J = 7.3 Hz, 1H), 6.80 (s, 1H), 6.11 (d, J = 8.1 Hz, 1H), 6.00 (d, J = 8.4 Hz, 1H), 2.98 (m, 4H), 2.25 (d, J = 0.8 Hz, 3H), 1.39 (d, J = 6.8 Hz, 6H), 1.32 (d, J = 6.8 Hz, 6H), 1.25 (dd, J = 10.4, 6.8 Hz, 12H). ^{13}C NMR (101 MHz, acetone) δ 158.29, 158.23, 154.94, 154.87, 145.53, 145.38, 138.28, 137.55, 131.58, 130.52, 125.92, 125.70, 124.92, 124.57, 123.92, 121.51, 119.39, 116.76, 115.04, 114.91, 112.40, 96.22, 28.83, 28.65, 24.75, 23.63, 23.52, 22.85, 20.48. Elemental analysis calculated C 69.13, H 6.22, N 7.68; found C 69.08, H 6.05, N 7.43.

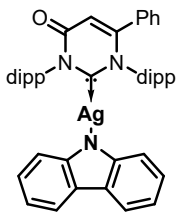

Ph-Ag was obtained with a yield of 79% as yellow powder. ^{1}H NMR (400 MHz, acetone) δ 7.85 – 7.70 (m, 4H), 7.60 (d, *J* = 7.8 Hz, 2H), 7.53 – 7.46 (m, 3H), 7.45 – 7.38 (m, 4H), 6.92 (ddd, *J* = 8.2, 7.0, 1.2 Hz, 2H), 6.87 (s, 1H), 6.78 – 6.69 (m, 2H), 6.02 (d, *J* = 8.1 Hz, 2H), 3.26 – 2.99 (m, 4H), 1.35 (d, *J* = 6.8 Hz, 6H), 1.29 (dd, *J* = 12.4, 6.8 Hz, 12H), 1.15 (d, *J* = 6.7 Hz, 6H). ^{13}C NMR (101 MHz, acetone) δ 158.21, 158.15, 156.44, 156.37, 150.29, 145.68, 145.56, 138.90, 137.54, 131.72, 131.32, 130.80, 130.48, 129.53, 128.31, 125.48, 124.93, 123.85, 122.76, 118.58, 114.55, 114.48, 113.61, 28.83, 28.81, 25.48, 23.88, 23.55, 22.24. Elemental analysis calculated C 72.06, H 6.31, N 5.48; found C 71.86, H 6.18, N 5.28.

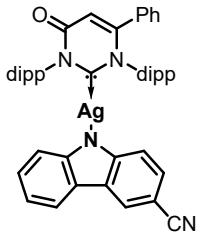

Ph-Ag^{CN} was obtained with a yield of 73% as light yellow powder. ^{1}H NMR (400 MHz, acetone) δ 8.20 (d, *J* = 1.3 Hz, 1H), 7.92 (d, *J* = 7.6 Hz, 1H), 7.86 (t, *J* = 7.8 Hz, 1H), 7.79 (t, *J* = 7.8 Hz, 1H), 7.63 (d, *J* = 7.8 Hz, 2H), 7.52 (d, *J* = 7.9 Hz, 2H), 7.50 – 7.47 (m, 1H), 7.46 – 7.38 (m, 4H), 7.20 (dd, *J* = 8.5, 1.7 Hz, 1H), 7.07 (ddd, *J* = 8.2, 7.0, 1.2 Hz, 1H), 6.94 – 6.86 (m, 2H), 6.09 (d, *J* = 8.2 Hz, 1H), 6.02 – 5.95 (m, 1H), 3.21 – 3.04 (m, 4H), 1.34 (d, *J* = 6.8 Hz, 6H), 1.28 (dd, *J* = 8.4, 6.8 Hz, 12H), 1.15 (d, *J* = 6.7 Hz, 6H). ^{13}C NMR (101 MHz, acetone) δ 158.14, 158.09, 156.35, 145.76, 145.68, 139.00, 137.62, 131.62, 131.46, 130.87, 130.63, 129.52, 128.35, 125.67, 125.59, 125.03, 124.54, 123.90, 121.52, 119.38, 116.73, 115.08, 114.95, 113.79, 96.19, 28.81, 28.78, 25.53, 23.89, 23.57, 22.22. Elemental analysis calculated C 71.30, H 5.98, N 7.08; found C 71.08, H 5.97, N 7.03.

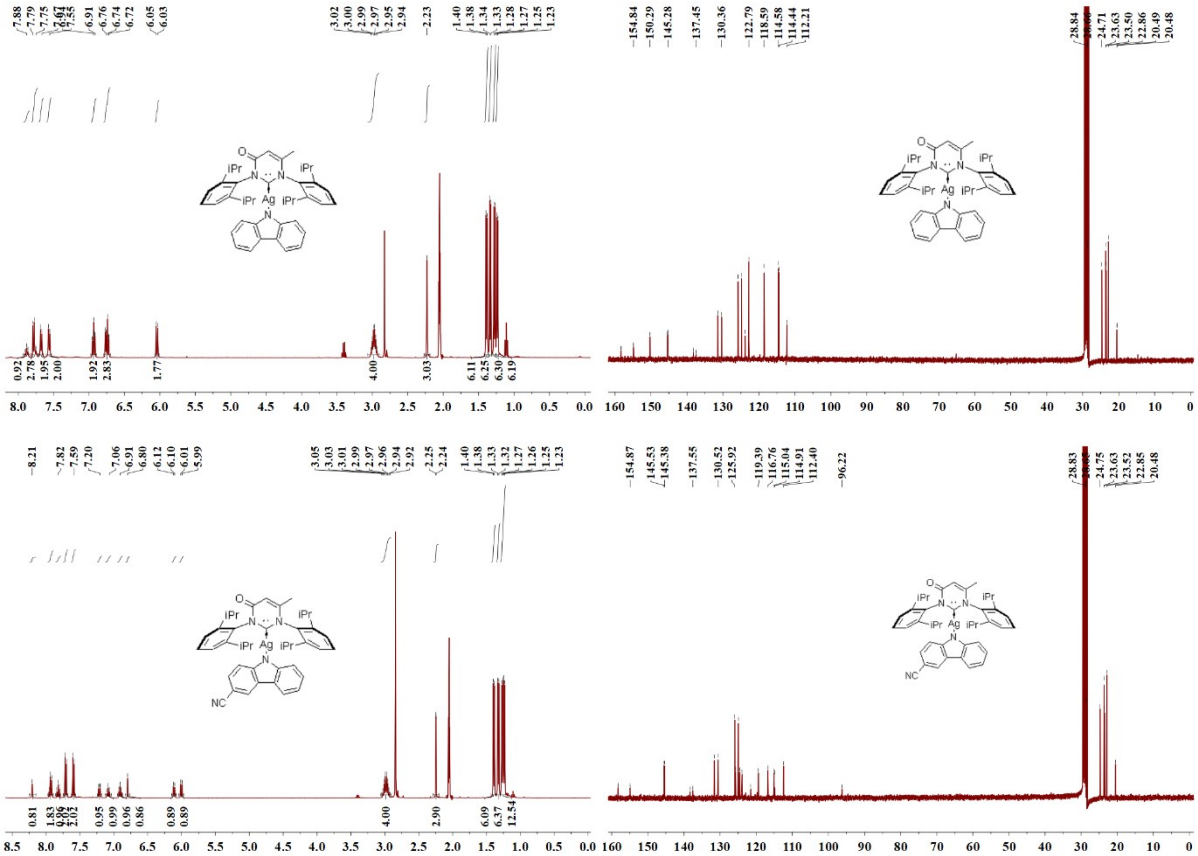

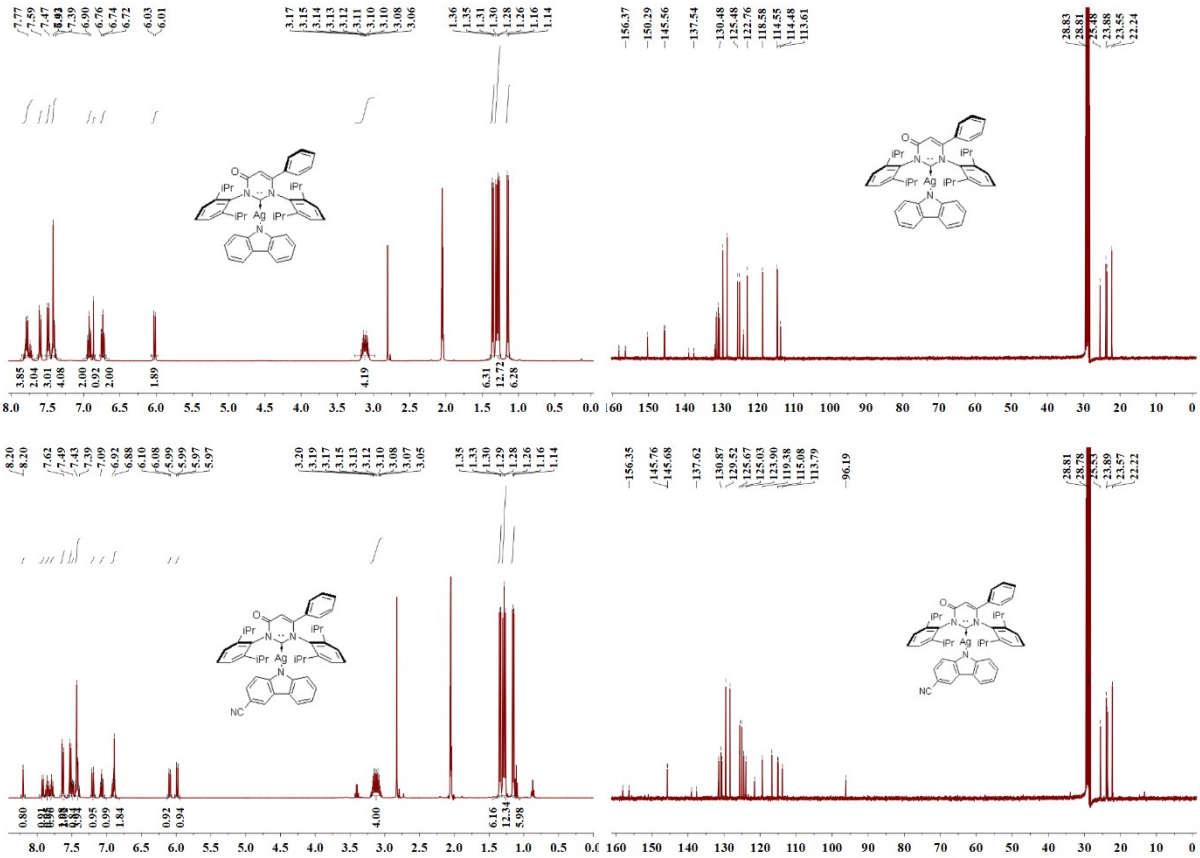

Figure S3 ^{1}H NMR and ^{13}C NMR spectra of the Ag(I) complexes

Synthesis of the Au complexes

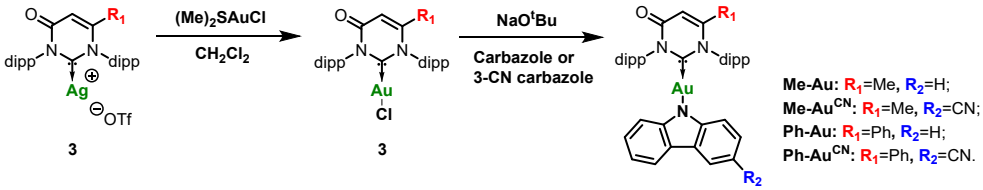

The Au(I)-Cl intermediate complexes were obtained by a metal ion exchange reaction. Equal equivalent of Carbene-AgOTf and $(Me)_2SAuCl$ were stirred in anhydrous CH_2Cl_2 for overnight. After the filtration through Celite, the filtrate was dried under vacuum. Excess amount of ether was added in the raw material and the intermediate complex was obtained as light purple precipitate (yield over 90%), which was used in the following reactions without further purifications.

Me-Au, **Me-Au** ^{CN}, **Ph-Au** and **Ph-Au** ^{CN} were synthesized according to a known procedure which was well described in previous publications.[3-5]

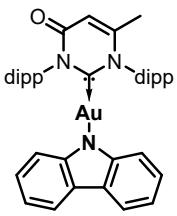

Me-Au was obtained with a yield of 80% as orange powder. ^{1}H NMR (400 MHz, acetone) δ 7.90 (t, J = 7.8 Hz, 1H), 7.82 – 7.75 (m, 3H), 7.67 (d, J = 7.8 Hz, 2H), 7.56 (d, J = 7.8 Hz, 2H), 6.95 (ddd, J = 8.2, 7.0, 1.3 Hz, 2H), 6.82 – 6.75 (m, 3H), 6.08 (dt, J = 8.2, 0.9 Hz, 2H), 3.02 – 2.88 (m, 4H), 2.22 (d, J = 1.0 Hz, 3H), 1.39 (dd, J = 6.8, 5.7 Hz, 12H), 1.30 (d, J = 6.9 Hz, 6H), 1.23 (d, J = 6.8 Hz, 6H). ^{13}C NMR (101 MHz, acetone) δ 201.36, 158.40, 155.16,

149.16, 145.44, 145.33, 137.11, 136.05, 131.11, 130.01, 125.41, 124.37, 123.59, 122.82, 118.41, 115.63, 113.79, 111.05, 28.74, 28.57, 24.09, 23.39, 23.05, 22.81, 20.30. Elemental analysis calculated C 62.04, H 5.84, N 5.29; found C 61.97, H 5.68, N 5.18.

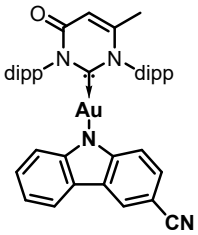

Me-Au^{CN} was obtained with a yield of 78% as yellow powder. ^{1}H NMR (400 MHz, acetone) δ 8.22 (dd, *J* = 1.7, 0.6 Hz, 1H), 7.93 (dd, *J* = 11.1, 4.5 Hz, 2H), 7.82 (t, *J* = 7.8 Hz, 1H), 7.69 (d, *J* = 7.8 Hz, 2H), 7.60 – 7.54 (m, 2H), 7.22 (dd, *J* = 8.5, 1.7 Hz, 1H), 7.08 (ddd, *J* = 8.2, 7.1, 1.2 Hz, 1H), 6.93 (ddd, *J* = 7.9, 7.1, 1.0 Hz, 1H), 6.80 (d, *J* = 1.0 Hz, 1H), 6.13 (dt, *J* = 8.2, 0.8 Hz, 1H), 6.05 (dd, *J* = 8.5, 0.6 Hz, 1H), 3.01 – 2.86 (m, 4H), 2.22 (d, *J* = 1.0 Hz, 3H), 1.37 (dd, *J* = 6.8, 1.4 Hz, 12H), 1.28 (d, *J* = 6.8 Hz, 6H), 1.22 (d, *J* = 6.8 Hz, 6H). ^{13}C NMR (101 MHz, acetone) δ 200.52, 158.44, 155.37, 151.13, 150.04, 145.74, 145.61, 137.31, 136.24, 131.50, 130.41, 125.89, 125.72, 124.71, 124.67, 124.02, 123.96, 123.07, 121.07, 119.42, 117.72, 114.54, 114.51, 111.60, 97.71, 24.30, 23.59, 23.25, 23.01, 20.49. Elemental analysis calculated C 61.61, H 5.54, N 6.84; found C 61.88, H 5.53, N 6.75.

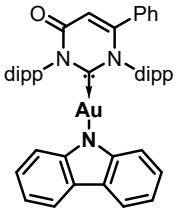

Ph-Au was obtained with a yield of 82% as orange powder. ^{1}H NMR (400 MHz, acetone) δ 7.85 – 7.71 (m, 4H), 7.58 (d, *J* = 7.8 Hz, 2H), 7.50 – 7.42 (m, 3H), 7.38 (d, *J* = 4.4 Hz, 4H), 6.93 (ddd, *J* = 8.2, 7.0, 1.3 Hz, 2H), 6.86 (s, 1H), 6.77 (ddd, *J* = 7.9, 7.1, 1.0 Hz, 2H), 6.05 (dt, *J* = 8.2, 0.8 Hz, 2H), 3.07 (sept, *J* = 6.7 Hz, 4H), 1.41 (d, *J* = 6.8 Hz, 6H), 1.32 (d, *J* = 6.8 Hz, 6H), 1.26 (d, *J* = 6.8 Hz, 6H), 1.11 (d, *J* = 6.7 Hz, 6H). ^{13}C NMR (101 MHz, acetone) δ 202.37, 158.56, 156.94, 149.36, 146.07, 145.78, 137.84, 136.36, 131.70, 131.26, 130.80, 130.32, 129.73, 128.27, 125.30, 124.70, 123.81, 123.02, 118.62, 115.84, 114.05, 112.78, 25.02, 23.81, 23.37, 22.47. Elemental analysis calculated C 64.55, H 5.65, N 4.91; found C 64.40, H 5.64, N 4.90.

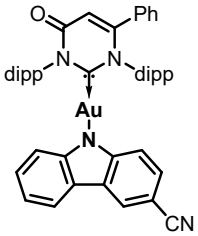

Ph-Au^{CN} was obtained with a yield of 80% as yellow powder. ^{1}H NMR (400 MHz, acetone) δ 8.23 (dd, *J* = 1.7, 0.6 Hz, 1H), 7.97 – 7.92 (m, 1H), 7.84 (dt, *J* = 20.4, 7.8 Hz, 2H), 7.62 (d, *J* = 7.8 Hz, 2H), 7.54 – 7.45 (m, 3H), 7.41 (d, *J* = 4.3 Hz, 4H), 7.22 (dd, *J* = 8.5, 1.7 Hz, 1H), 7.08 (ddd, *J* = 8.3, 7.1, 1.3 Hz, 1H), 6.94 (ddd, *J* = 8.0, 7.1, 1.0 Hz, 1H), 6.91 (s, 1H), 6.13 (dd, *J* = 8.2, 0.8 Hz, 1H), 6.05 (dd, *J* = 8.5, 0.6 Hz, 1H), 3.18 – 3.00 (m, 4H), 1.42 (d, *J* = 6.8 Hz, 6H), 1.32 (d, *J* = 6.8 Hz, 6H), 1.27 (d, *J* = 6.8 Hz, 6H), 1.13 (d, *J* = 6.7 Hz, 6H). ^{13}C NMR (101 MHz, acetone) δ 201.38, 158.39, 156.87, 151.12, 150.03, 146.13, 145.87, 137.87, 136.35, 131.57, 131.42, 130.86, 130.50, 129.72, 128.28, 125.87, 125.40, 124.78, 124.69, 124.03, 123.95, 123.08, 121.07, 119.41, 117.70, 114.58, 114.57, 113.10, 97.69, 25.03, 23.79, 23.34, 22.44. Elemental analysis calculated C 64.09, H 5.38, N 6.36; found C 63.79, H 5.44, N 6.33.

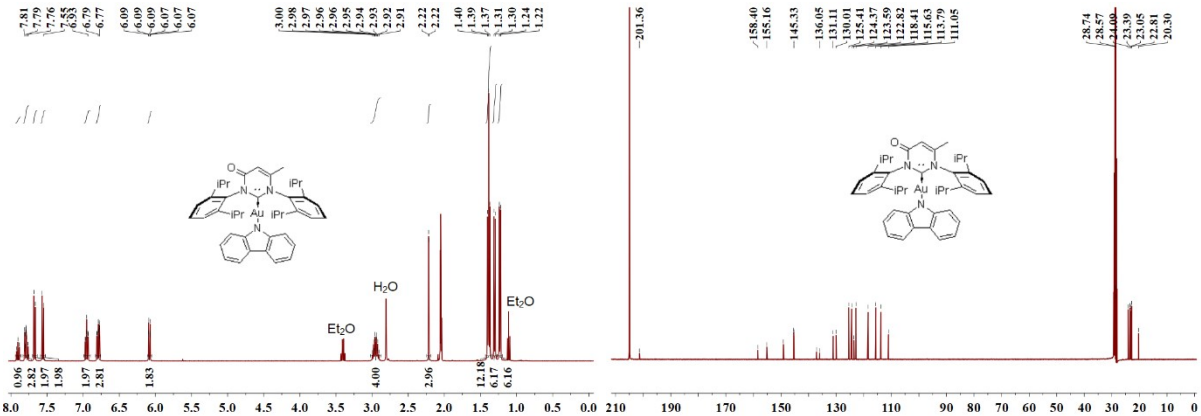
Et2O
H2O
Et2O

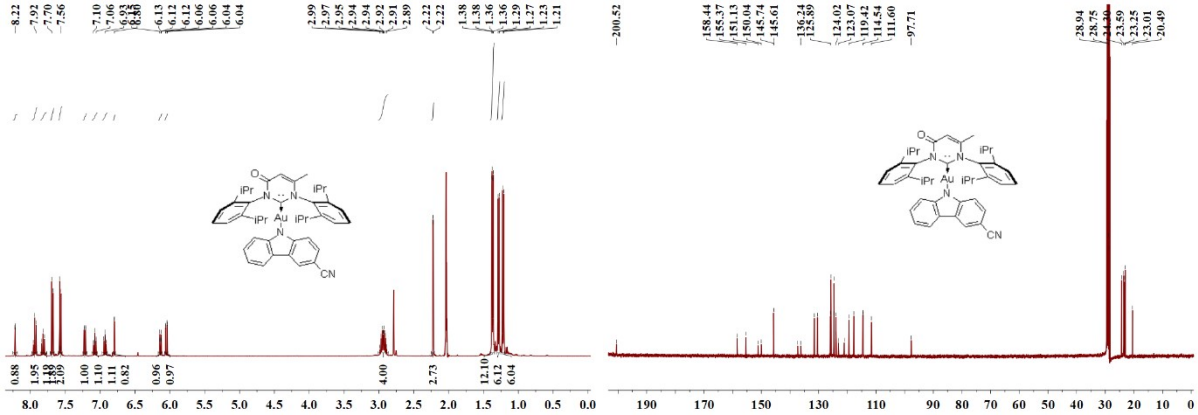

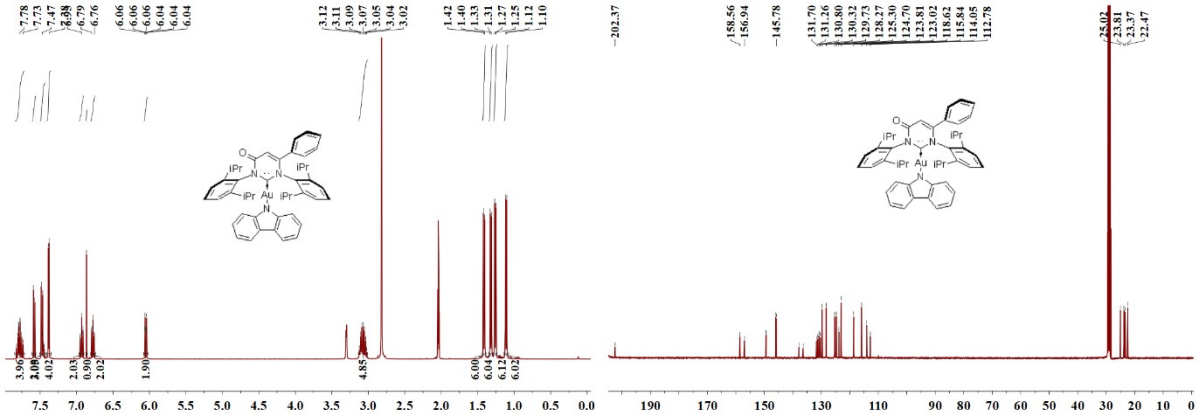

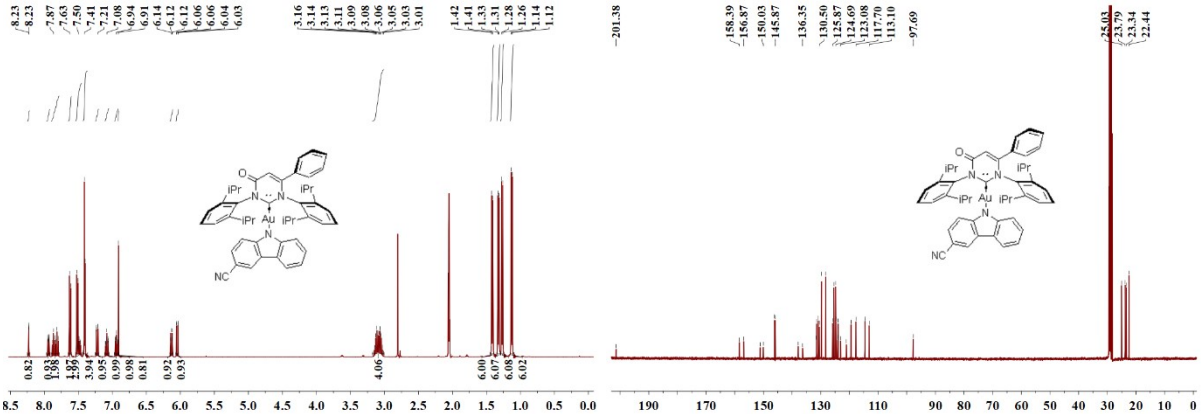

Figure S4 ^{1}H NMR and ^{13}C NMR spectra of the Au(I) complexes

Crystallography

All single crystal samples suitable for X-ray diffraction measurements were grown by slow diffusion of ether into CH_2Cl_2 solution. The diffraction intensity frames were collected on a Bruker APEX DUO 3-circle platform diffractometer using Cu Kα radiation (λ=1.54184 Å). The diffractometer was equipped with an APEX II CCD detector and an Oxford Cryosystems Cryostream 700 apparatus for low-temperature data collection adjusted to 100(2) K. The single crystal structures for MeCu was determined at 100 K with a Rigaku Xta LAB Synergy S, equipped with an HyPix-600HE detector and an Oxford Cryostream 800 low-temperature unit, using a Cu K_α PhotonJet-S X-ray radiation source. The crystal was mounted in a Cryo-Loop using Paratone oil. The frames were integrated using the SAINT algorithm to give the hkl files. Data were corrected for absorption effects using the multiscan method (SADABS). The structures were solved by intrinsic phasing and refined with the Bruker SHELXTL software package or Rigaku Crysalis pro Software respectively. Supplementary crystallographic data can be downloaded from Cambridge Crystallographic Data Center (CCDC) with the following registration numbers: **Me-Cu** (2117673 or RARFID); **Me-Ag** (2117674 or RARFOJ); **Ph-Au** (2117675 or RARFEZ); **Ph-Au^{CN}** (2117672 or RARFAV).

Table S1 Crystallographic data of Me-Cu, Me-Ag, Ph-Au and Ph-Au^{CN}

Complex	**Me-Cu**	**Me-Ag**	**Ph-Au**	**Ph-Au^{CN}**
Formula	$C_{41}H_{46}CuN_3O$	$C_{41}H_{46}AgN_3O$	$C_{46}H_{48}AuN_3O$	$C_{47}H_{47}AuN_4O$
Formula weight	659.84	706.0	855.84	880.85
Temperature	100 K	100 K	100 K	100 K
Wavelength	1.54184 Å	1.54184 Å	1.54184 Å	1.54184 Å
Crystal system	orthorhombic	orthorhombic	orthorhombic	monoclinic
Space group	Pna2$_1$	Pna2$_1$	$P2_12_12_1$	$I2/a$
a (Å)	23.6479(3)	24.3212(3)	9.113(5)	26.0430(3)
b (Å)	8.7894(1)	8.7335(1)	13.346(5)	8.55063(8)
c (Å)	36.5241(7)	36.2832(4)	33.166(16)	39.0005(4)
α (deg)	90	90	90	90
β (deg)	90	90	90	108.1204(11)
γ (deg)	90	90	90	90
Volume (Å^3)	7591.5(2)	7706.8(2)	4034(3)	8254.07(15)
Z	8	8	4	8
F (000)	2796	2950	1728	3552
θ (deg) for collection	5.18 to 160.56	4.87 to 155.34	5.35 to 69.60	2.38 to 77.91
Index range	-30≤h≤26 -10≤k≤11 -46≤l≤44	-30≤h≤27 -10≤k≤10 --45≤l≤44	-11≤h≤11 -16≤k≤15 -38≤l≤40	-32≤h≤31 -10≤k≤10 -45≤l≤49
Reflections measured	60363	51974	50861	29356
Goodness of Fit	1.035	1.053	1.069	1.074
Final R indices [$I > 2\sigma$(I)]	R_1= 0.0868 wR_2= 0.2094	R_1= 0.0618 wR_2= 0.1555	R_1= 0.0151 wR_2= 0.0377	R_1= 0.0201 wR_2= 0.0480
R indices (all data)	R_1= 0.0933 wR_2= 0.2137	R_1= 0.0631 wR_2= 0.1564	R_1= 0.0153 wR_2= 0.0378	R_1= 0.0224 wR_2= 0.0488
CCDC number	2117673	2117674	2117675	2117672

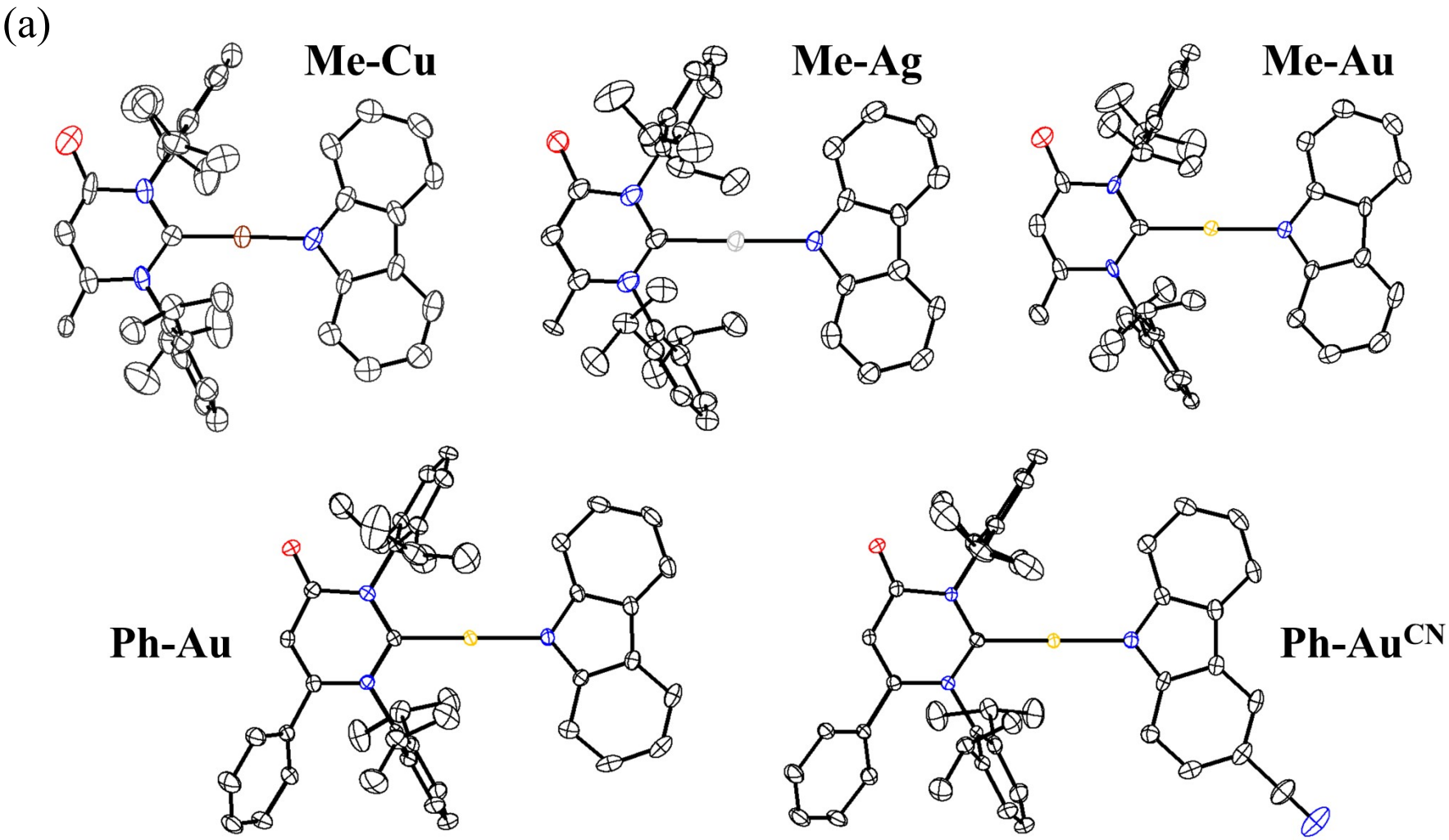

Figure S5 Thermal Ellipsoid diagrams (a) and packing diagrams (b) of Me-Cu, Me-Ag, Ph-Au and Ph-Au^{CN}

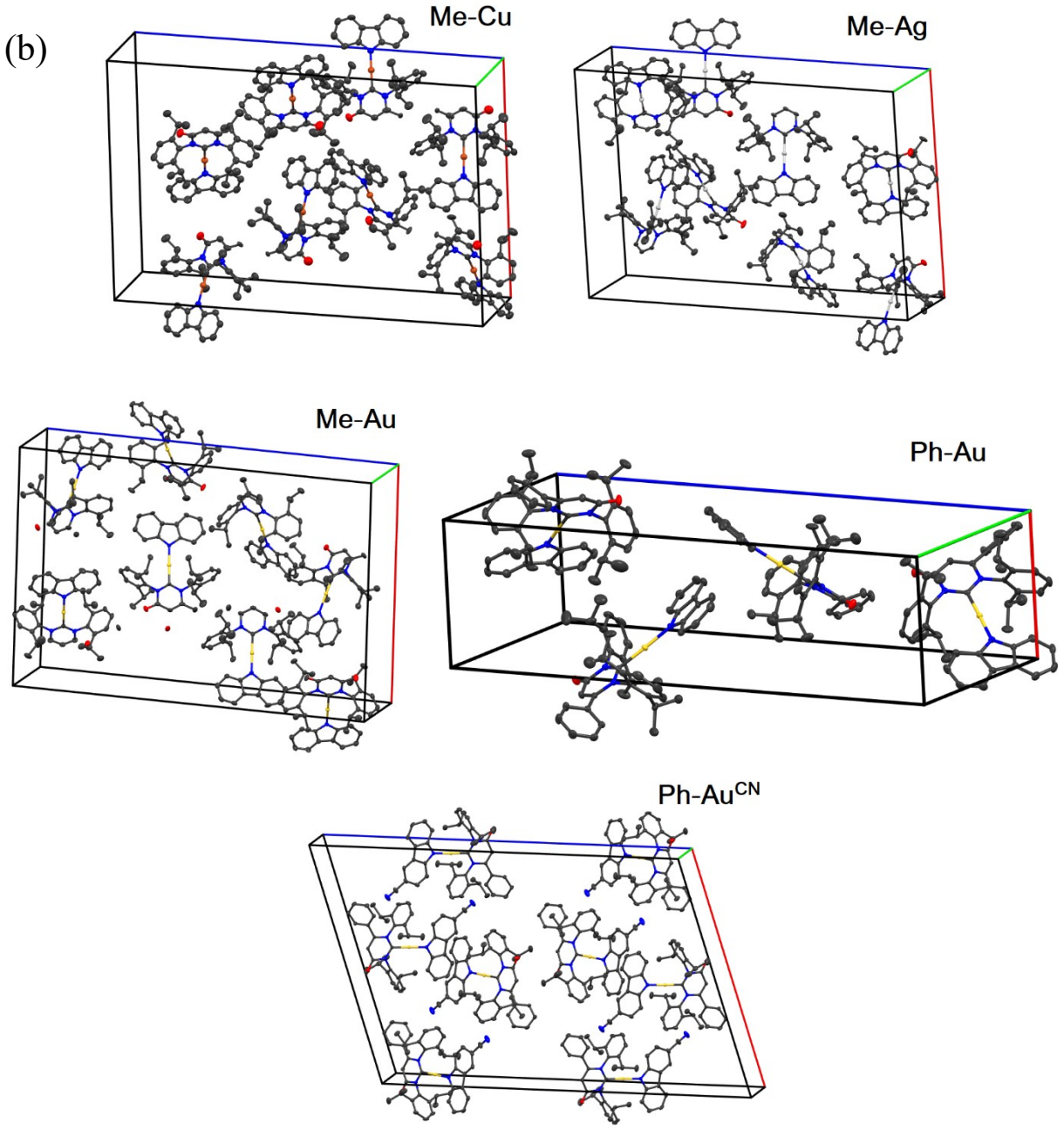

Figure S5 Thermal Ellipsoid diagrams (a) and packing diagrams (b) of Me-Cu, Me-Ag, Ph-Au and Ph-Au^{CN} (continued)

Electrochemistry

Cyclic voltammetry (CV) and differential pulsed voltammetry (DPV) were performed using a VersaSTAT 3 potentiostat in anhydrous DMF under N_2 atmosphere. A standard three-electrode system with a glassy carbon rod working electrode, a platinum wire counter electrode and a silver wire reference electrode was employed. Tetra-*n*-butyl ammonium hexafluorophosphate (TBAHF) was used as supporting electrolyte on a concentration of 0.1M. Ferrocene was used as internal reference and the redox potentials of the complexes were adjusting the ferrocene redox potentials as 0V.

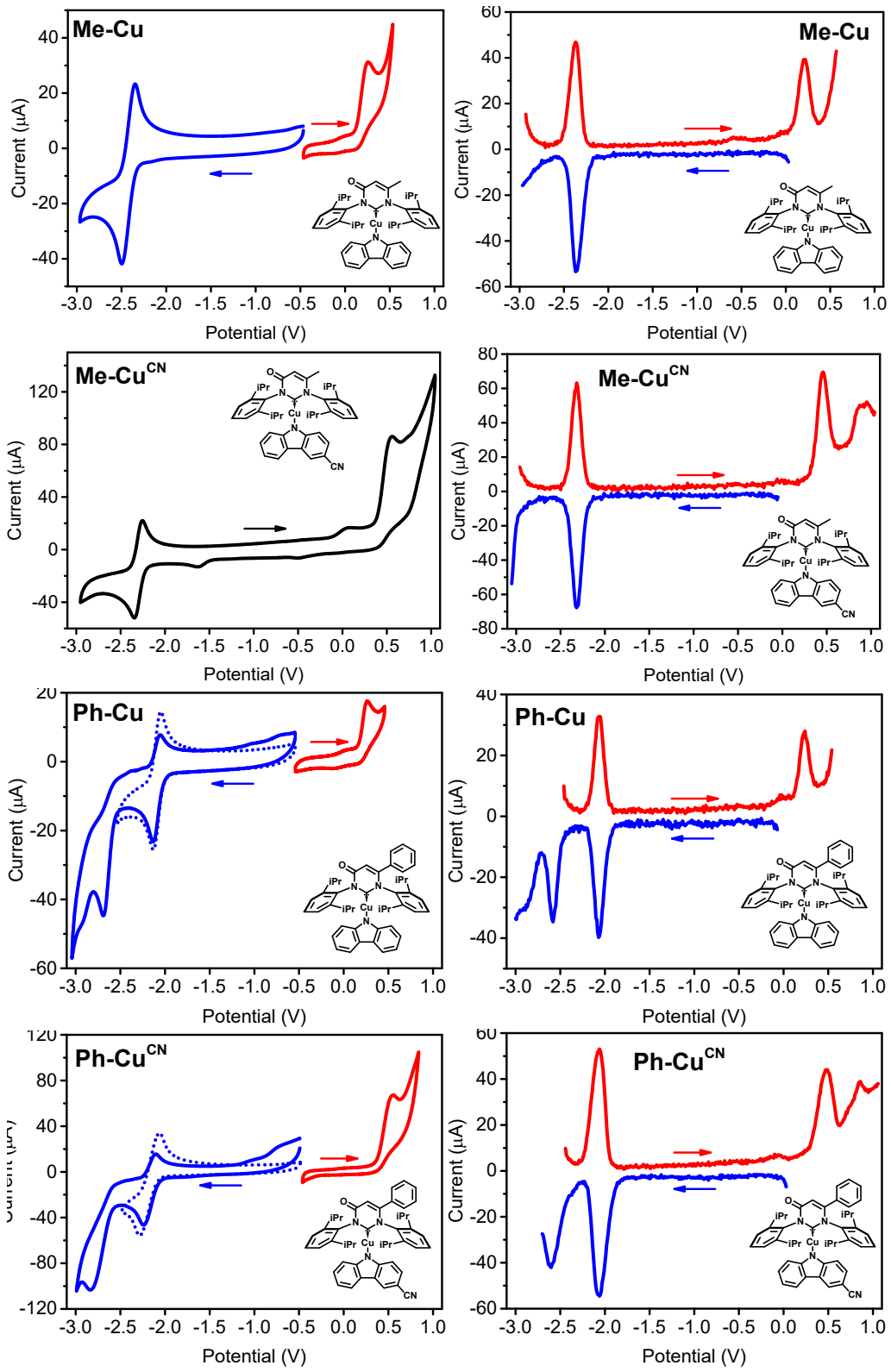

Figure S6 CV and DPV curves for (carbene)Cu(carbazolyl) in DMF

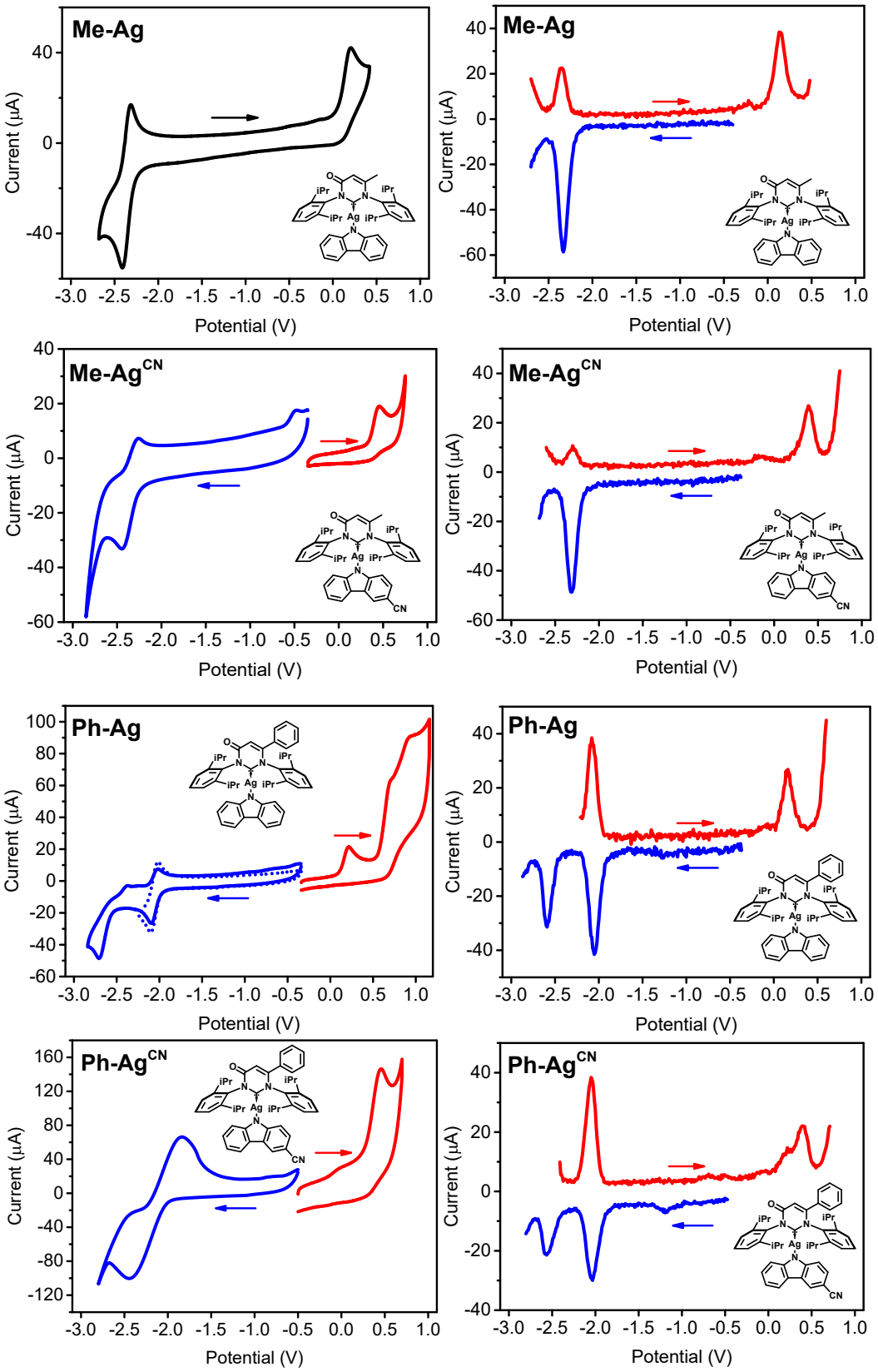

Figure S7 CV and DPV curves for (carbene)Ag(carbazolyl) in DMF

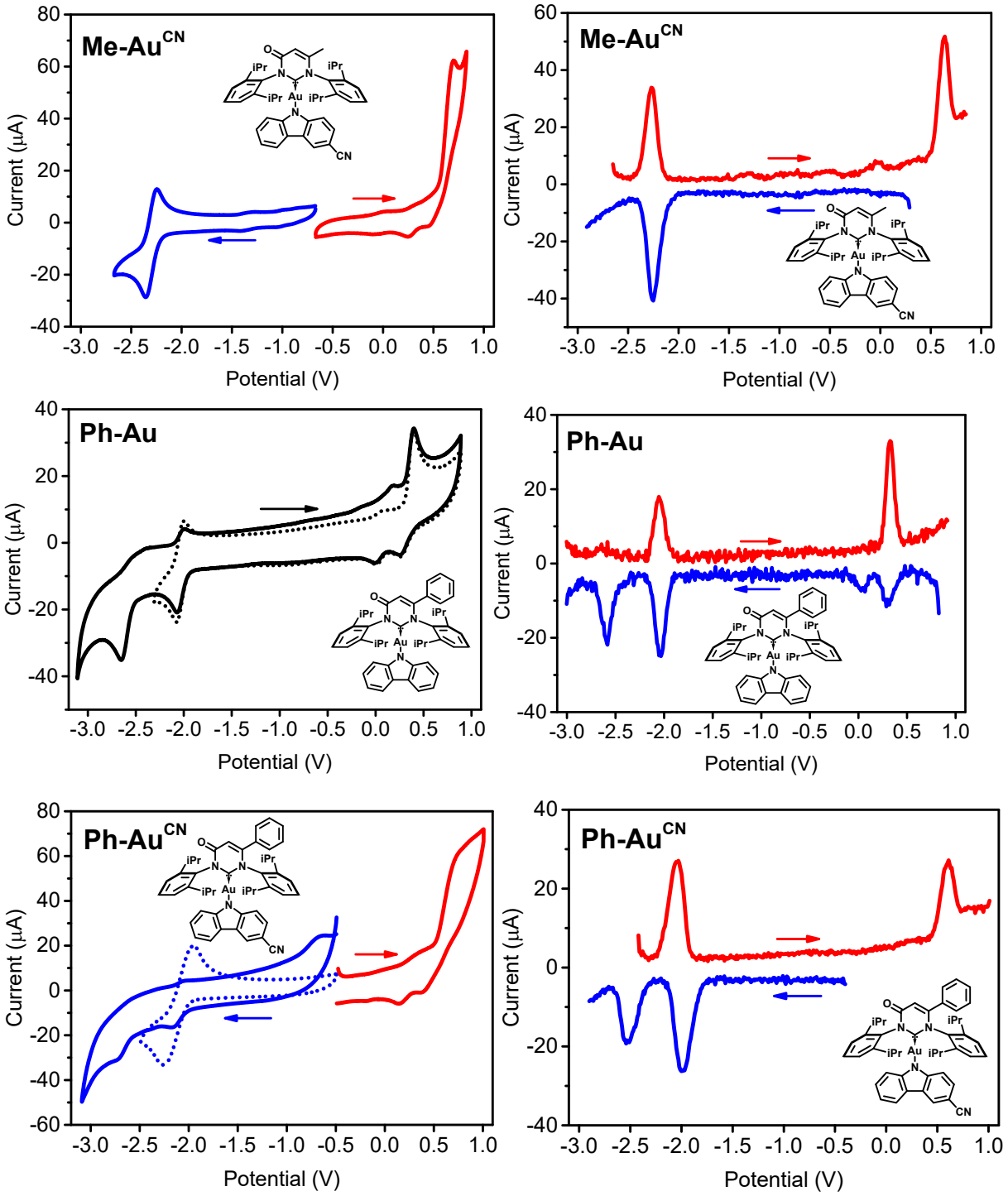

Figure S8 CV and DPV curves for (carbene)Au(carbazolyl) in DMF

Table S2 Electrochemical data of the coinage metal complexes

Complex	**Me-Cu**	**Me-Cu^{CN}**	**Ph-Cu**	**Ph-Cu^{CN}**
E_{ox}[a]	0.21	0.46	0.24	0.48
E_{red}[a]	-2.37	-2.32	-2.07, -2.58	-2.06, -2.60
$E_{ox\text{-}red}$[b]	2.58	2.78	2.31	2.54
Complex	**Me-Ag**	**Me-Ag^{CN}**	**Ph-Ag**	**Ph-Ag^{CN}**
E_{ox}[a]	0.14	0.39	0.16	0.40
E_{red}[a]	-2.33	-2.31	-2.05, -2.59	-2.03, -2.56
$E_{ox\text{-}red}$[b]	2.47	2.70	2.21	2.43
Complex	**Me-Au**[c]	**Me-Au^{CN}**	**Ph-Au**	**Ph-Au^{CN}**
E_{ox}[a]	0.33	0.62	0.32	0.60
E_{red}[a]	-2.31	-2.25	-2.04, -2.59	-2.00, -2.53
$E_{ox\text{-}red}$[b]	2.64	2.87	2.36	2.60

[a] Potential values were obtained from DPV measurement using ferrocene/ferrocenium as internal reference whose potentials were adjusted as 0V; [b] The first reduction potential was used to calculated the gap when two reductions were observed; [c] Known data from reference[6]

Molecular modeling

All the theoretical calculations were carried out using Q-Chem 5.1 program as in gas phase and visualized using IQmol software. The ground state molecular geometries were optimized at the B3LYP/LACVP* level, followed by the TD-DFT calculations based on the optimized structures at the CAM-B3LYP/LACVP* level, aiming for the insight of vertical transitions. The geometries of the calculated structures were verified as true minima by vibrational analysis. The CAM-B3LYP functional ($\Omega = 0.17$) was found to replicate absorptions energies for the ^{1}ICT transitions in these derivatives. Details of NTOs were obtained by another TD-DFT calculations at the same level, and the NTO overlap values were calculated using the NTOverlap software written by Dr. Daniel Sylvinson as described in the supporting information of previous publication.[7] All the plots are provided with hydrogen atoms omitted for clarity. Isovalues for the NTO contours were set to 0.100.

Table S3 Plots of the frontier molecular orbitals

Complex	HOMO	LUMO	LUMO+1
Me-Cu	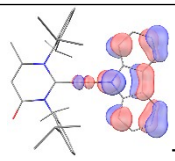 -4.22eV	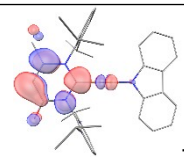 -1.99eV	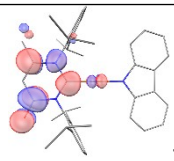 -1.58eV
Me-Cu^{CN}	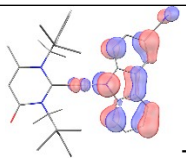 -4.71eV	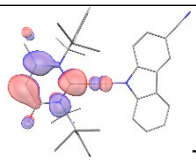 -2.20eV	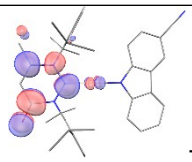 -1.80eV
Ph-Cu	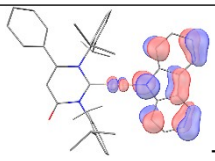 -4.19eV	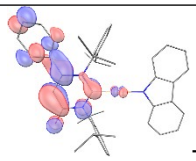 -2.26eV	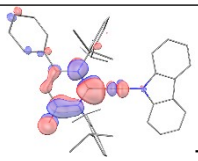 -1.69eV
Ph-Cu^{CN}	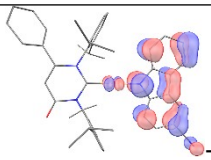 -4.68eV	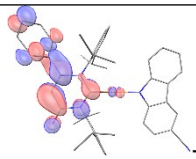 -2.45eV	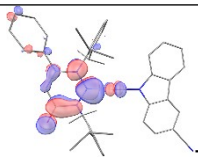 -1.90eV
Me-Ag	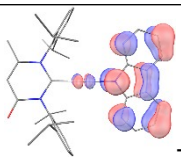 -4.11eV	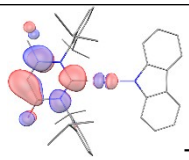 -2.07eV	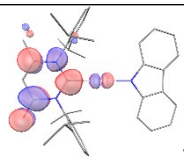 -1.69eV
Me-Ag^{CN}	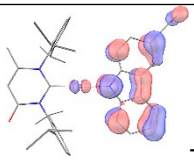 -4.63eV	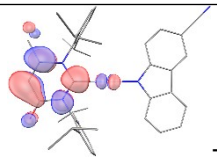 -2.26e V	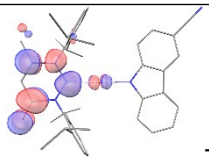 -1.88eV
Ph-Ag	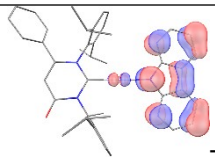 -4.08eV	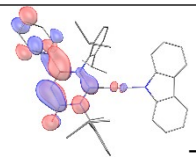 -2.37eV	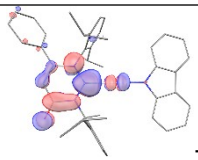 -1.74eV

Ph-Ag^{CN}	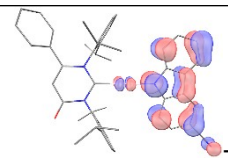 -4.57eV	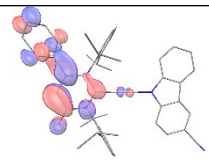 -2.53eV	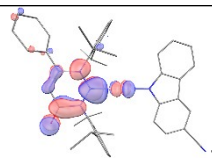 -1.93eV
Me-Au	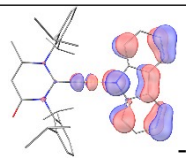 -4.38eV	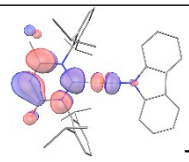 -1.99eV	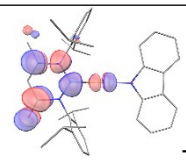 -1.61eV
Me-Au^{CN}	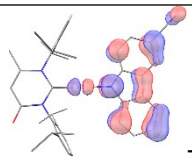 -4.84eV	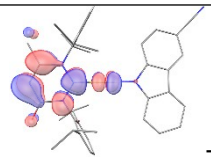 -2.20eV	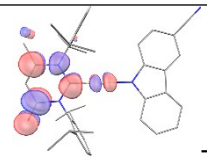 -1.82eV
Ph-Au	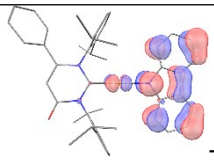 -4.35eV	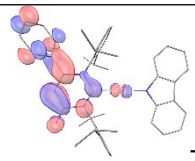 -2.26eV	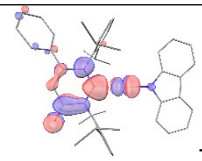 -1.69eV
Ph-Au^{CN}	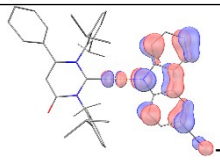 -4.82eV	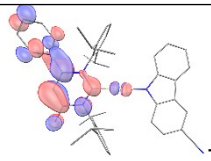 -2.48eV	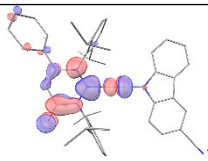 -1.90eV

Table S4 Calculated vertical transition properties of the S_1 and T_1 states

Complex	State	Energy (eV/nm)	Osc. strength	Major contribution
Me-Cu	S_1	2.40 / 517	0.1061	HOMO→LUMO (88%) HOMO→LUMO+1 (11%)
	T_1	2.17 / 571	0.0000	HOMO→LUMO (80%) HOMO→LUMO+1 (15%)
Me-Cu^{CN}	S_1	2.67 / 464	0.1110	HOMO→LUMO (88%) HOMO→LUMO+1 (10%)
	T_1	2.47 / 502	0.0000	HOMO→LUMO (81%) HOMO→LUMO+1 (13%)
Ph-Cu	S_1	2.28 / 544	0.0759	HOMO→LUMO (82%) HOMO→LUMO+1 (17%)
	T_1	2.10 / 591	0.0000	HOMO→LUMO (62%) HOMO→LUMO+1 (33%)
Ph-Cu^{CN}	S_1	2.58 / 481	0.0857	HOMO→LUMO (78%) HOMO→LUMO+1 (20%)
	T_1	2.43 / 510	0.0000	HOMO→LUMO (62%) HOMO→LUMO+1 (32%)
Me-Ag	S_1	2.34 / 530	0.0726	HOMO→LUMO (86%) HOMO→LUMO+1 (13%)
	T_1	2.23 / 556	0.0000	HOMO→LUMO (80%) HOMO→LUMO+1 (18%)
Me-Ag^{CN}	S_1	2.66 / 466	0.0759	HOMO→LUMO (86%)

				HOMO→LUMO+1 (13%)
	T_1	2.57 / 483	0.0000	HOMO→LUMO (81%) HOMO→LUMO+1 (16%)
Ph-Ag	S_1	2.20 / 564	0.0463	HOMO→LUMO (89%) HOMO→LUMO+1 (10%)
	T_1	2.12 / 585	0.0000	HOMO→LUMO (78%) HOMO→LUMO+1 (20%)
Ph-Ag^{CN}	S_1	2.54 / 488	0.0471	HOMO→LUMO (85%) HOMO→LUMO+1 (14%)
	T_1	2.48 / 500	0.0000	HOMO→LUMO (77%) HOMO→LUMO+1 (21%)
Me-Au	S_1	2.59 / 479	0.1647	HOMO→LUMO (89%) HOMO→LUMO+1 (10%)
	T_1	2.32 / 535	0.0000	HOMO→LUMO (81%) HOMO→LUMO+1 (15%)
Me-Au^{CN}	S_1	2.83 / 438	0.1619	HOMO→LUMO (88%) HOMO→LUMO+1 (10%)
	T_1	2.61 / 475	0.0000	HOMO→LUMO (82%) HOMO→LUMO+1 (13%)
Ph-Au	S_1	2.46 / 504	0.1136	HOMO→LUMO (85%) HOMO→LUMO+1 (14%)
	T_1	2.25 / 551	0.0000	HOMO→LUMO (63%) HOMO→LUMO+1 (33%)
Ph-Au^{CN}	S_1	2.73 / 454	0.1277	HOMO→LUMO (81%) HOMO→LUMO+1 (17%)
	T_1	2.55 / 486	0.0000	HOMO→LUMO (63%) HOMO→LUMO+1 (31%)

Table S5 Calculated singlet-triplet energy gaps

Complex	ΔE_{ST} (eV)	Complex	ΔE_{ST} (eV)	Complex	ΔE_{ST} (eV)
Me-Cu	0.23	**Me-Ag**	0.11	**Me-Au**	0.27
Me-Cu^{CN}	0.20	**Me-Ag^{CN}**	0.09	**Me-Au^{CN}**	0.22
Ph-Cu	0.18	**Ph-Ag**	0.08	**Ph-Au**	0.21
Ph-Cu^{CN}	0.15	**Ph-Ag^{CN}**	0.06	**Ph-Au^{CN}**	0.18

ΔE_{ST} is the energetic difference between the S_1 and T_1 states whose energies are obtained as the vertical transition energies from the TD-DFT calculations at CAM-B3LYP/LACVP* level

Table S6 Natural transition orbitals analyses of the S_1 and T_1 state

Complex	S1	T1
Me-Cu	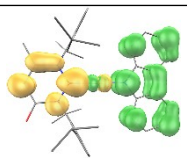 ICT (2.40eV, 98.9%)	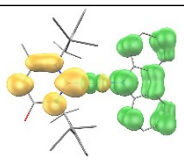 ICT (2.17eV, 99.0%)
Me-Cu^{CN}	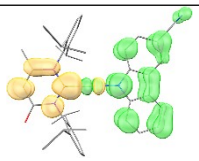 ICT (2.67eV, 99.1%)	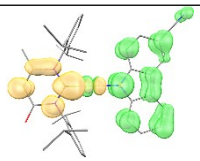 ICT (2.47eV, 98.5%)
Ph-Cu	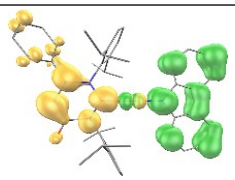 ICT (2.28eV, 99.3%)	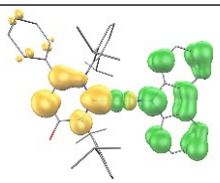 ICT (2.10eV, 99.0%)
Ph-Cu^{CN}	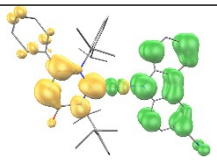 ICT (2.58eV, 99.4%)	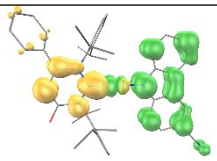 ICT (2.42eV, 98.4%)
Me-Ag	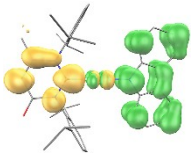 ICT (2.34eV, 99.4%)	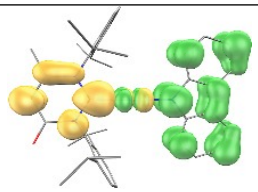 ICT (2.23eV, 99.4%)
Me-Ag^{CN}	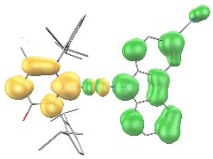 ICT (2.66eV, 99.6%)	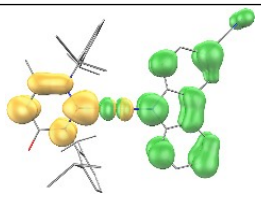 ICT (2.57eV, 98.9%)
Ph-Ag	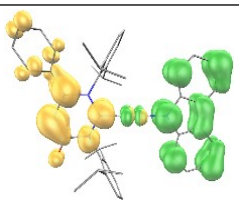 ICT (2.20eV, 99.8%)	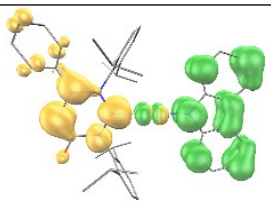 ICT (2.12eV, 99.6%)
Ph-Ag^{CN}	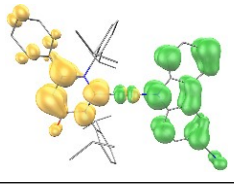 ICT (2.53eV, 99.7%)	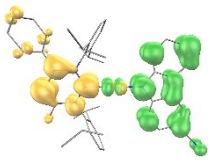 ICT (2.48eV, 99.2%)
Me-Au	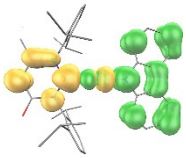 ICT (2.598eV, 98.7%)	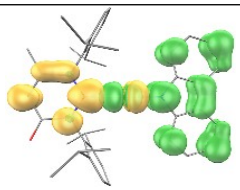 ICT (2.32eV, 98.6%)

Me-Au^{CN}	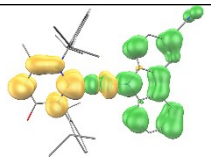 ICT (2.82eV, 98.9%)	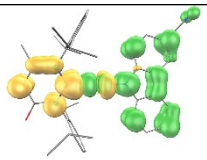 ICT (2.61eV, 97.6%)
Ph-Au	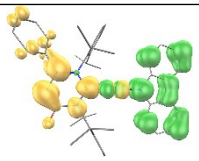 ICT (2.46eV, 99.1%)	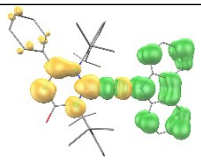 ICT (2.25eV, 98.6%)
Ph-Au^{CN}	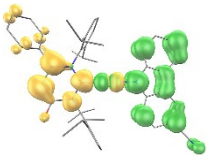 ICT (2.73eV, 99.2%)	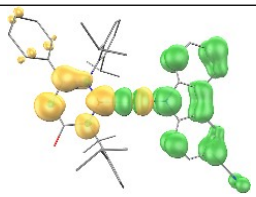 ICT (2.55eV, 97.4%)
Green for hole and yellow for electron		

Photophysics

Absorption spectra were recorded in dilute CH_2Cl_2 and toluene solution (around 5×10^{-5} mol/L) using a Hewlett-Packard 8453 diode array spectrometer. Steady state photoluminescent emission spectra were measured in dilute toluene at room temperature and in methyl cyclohexane (MeCy) at both room temperature and 77K on a Photon Technology International QuantaMaster model C-60 fluorimeter. Transient photoluminescent lifetimes were measured on an IBH Fluorocube instrument using time-correlated single-photon counting method (TCSPC) for those less than 100ms and multichannel scaling method (MSC) for those longer than 100ms. Photoluminescent quantum yields were determined using a Hamamatsu C9920 system equipped with a xenon lamp, calibrated integrating sphere and model C10027 photonic multichannel analyzer (PMA). Temperature-dependent lifetime measurements from 200 to 310 K were measured using IBH Fluorocube instrument in an OptistatDN Oxford cryostat. All fluid samples for luminescent measurements were deaerated by bubbling N_2. Doped polymer films (1wt%) were prepared in toluene solution of polystyrene (PS). The polymer solution with samples were dropcast onto a quartz substrate and the films were air-dried for 3h and completely dried under vacuum. The emission properties of polymer samples were measured under a stream of N2 during the measurements.

Strickler Berg analysis of radiative rates.

Strickler-Berg analysis, which has been proven successful for organic fluorophores, takes extinction spectral data to estimate oscillator strength for the transition between ground state and the first singlet excited state. Then, radiative decay rate for emission can be predicted in turn. The analysis requires the following data: absorption maximum in wavenumbers, integrated area of the S_0-S_1 transition in wavenumbers and the extinction coefficient in L mol^{-1} cm^{-1}. Here, the integrated area is estimated by integrating half of the low energy ICT absorption band and double it numerically aiming to avoiding the overlap with the high-energy ligand-based absorption. The equation used is shown below:

$$k_{fl} = 2.88 \times 10^{-9} \vartheta_0^2 \int \varepsilon d\vartheta$$

Where k_{fl} is the predicted radiative decay rate, ϑ_0 is the wavenumber of the absorption maximum, ε is the molar extinction coefficient.

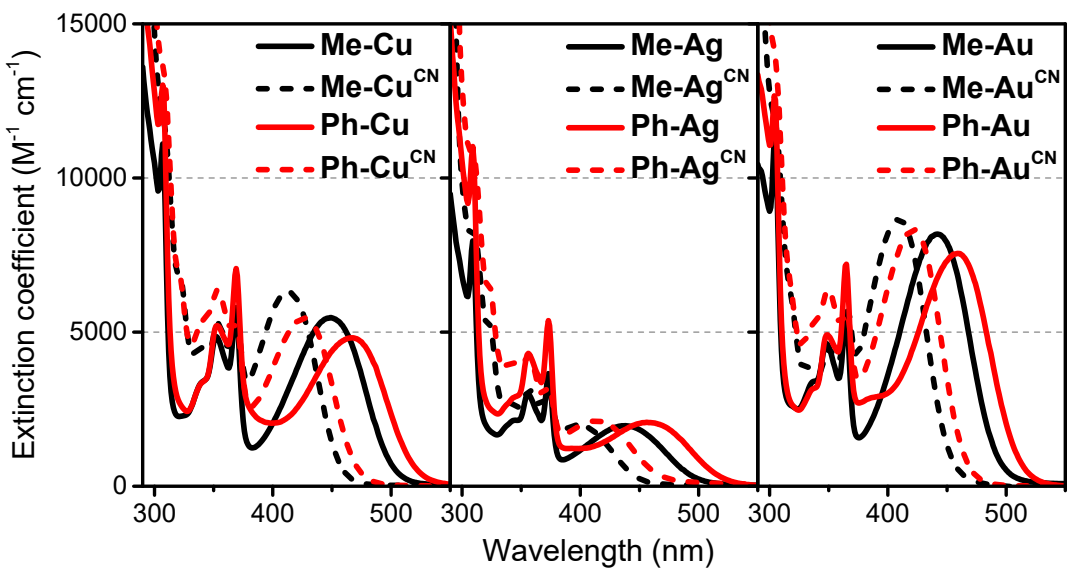

Figure S9 Absorption spectra of all the complexes in toluen

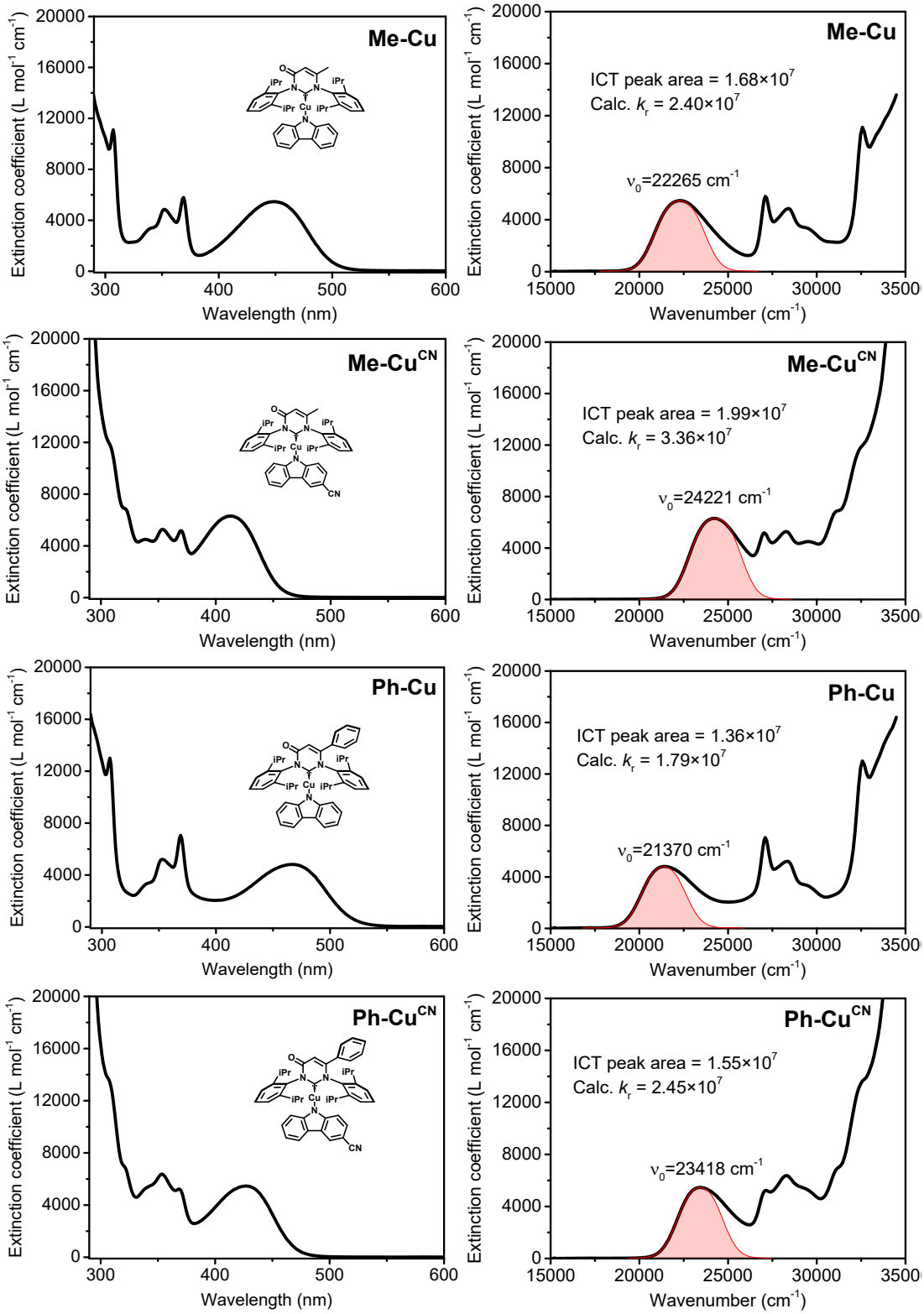

Figure S10 Absorption spectra in toluene and the theoretical calculations of k_r based on the Strickler-Berg equation for (carbene)Cu(carbazolyl) complexes.

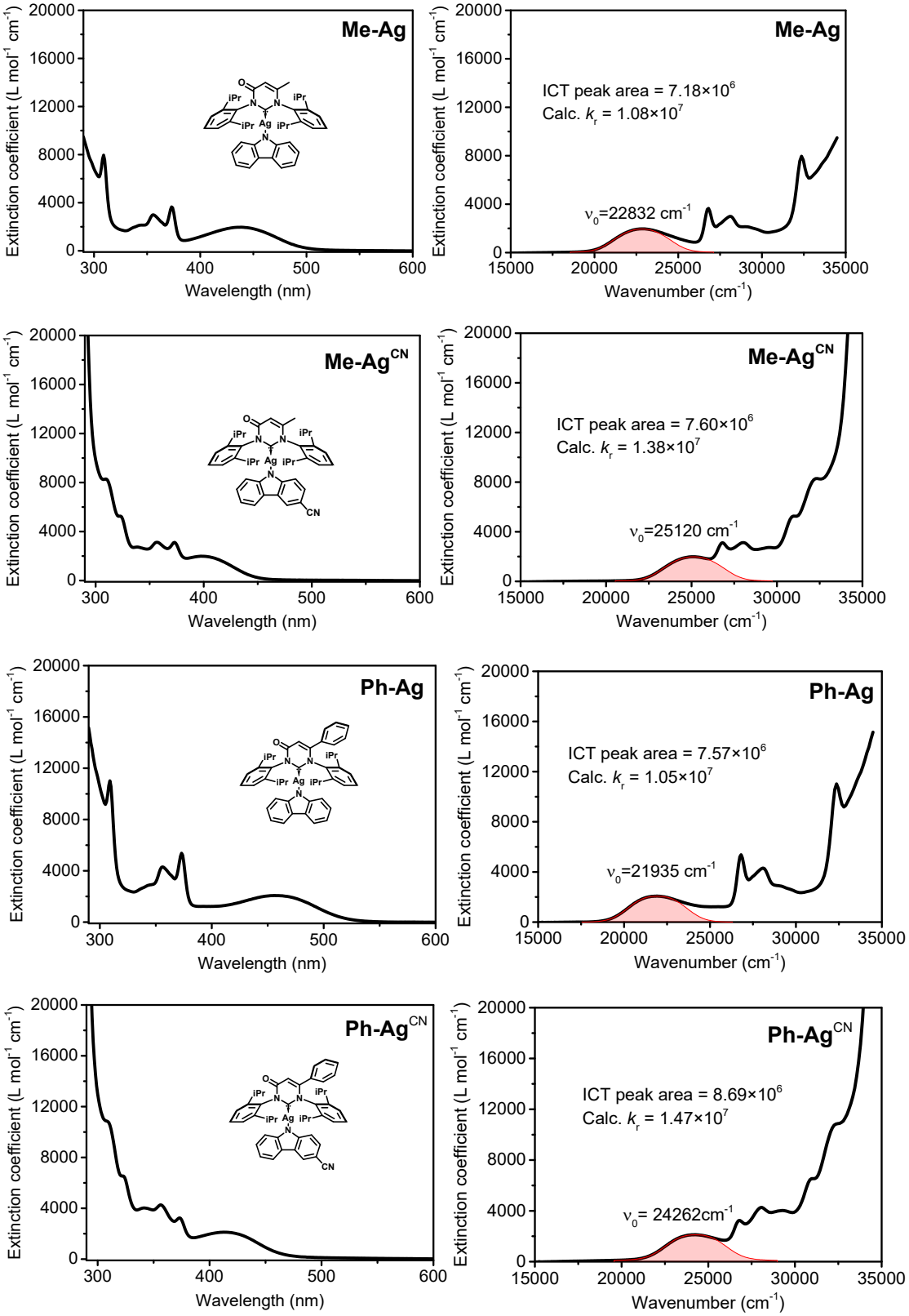

Figure S11 Absorption spectra in toluene and the theoretical calculations of k_r based on the Strickler-Berg equation for (carbene)Ag(carbazolyl) complexes.

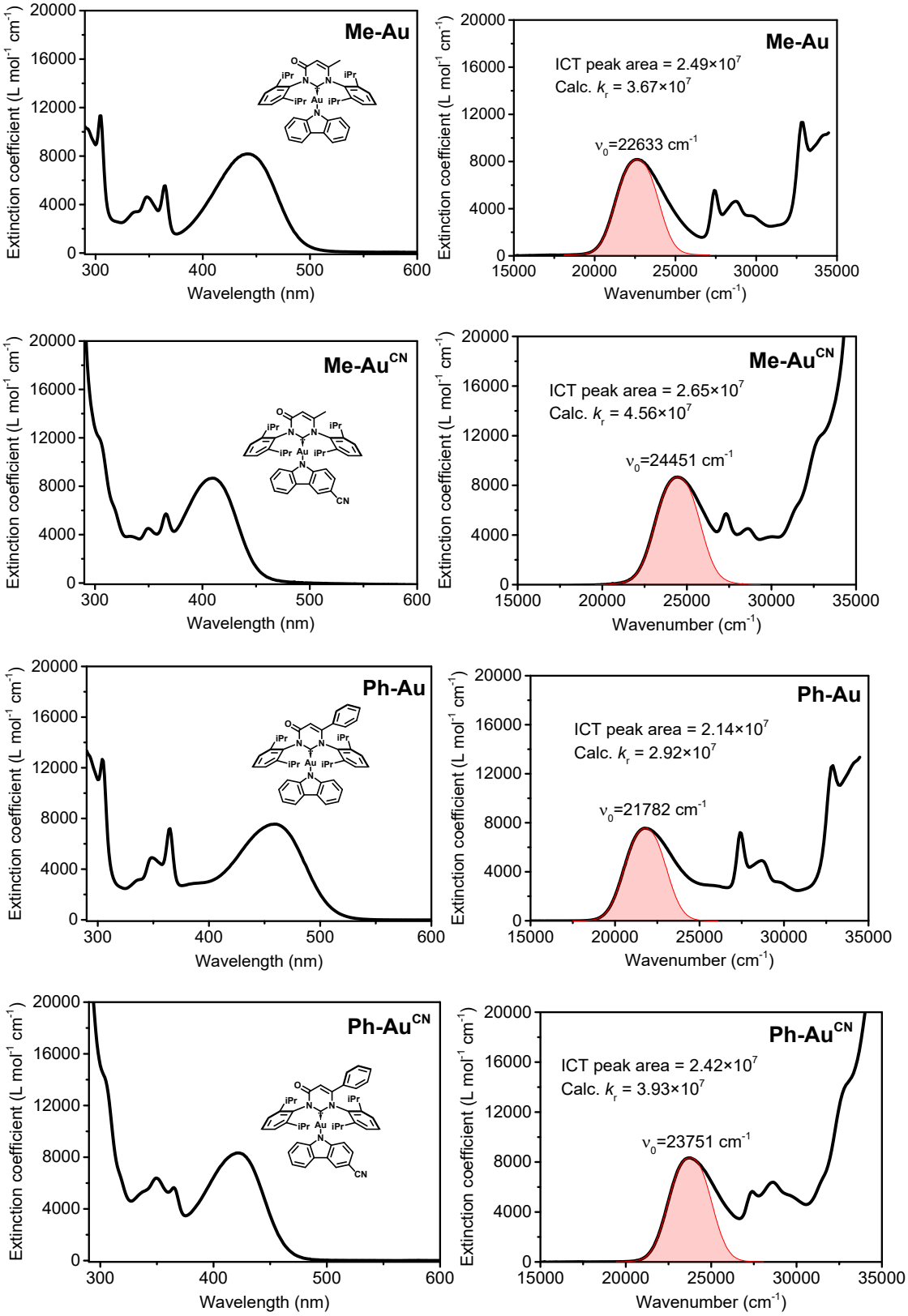

Figure S12 Absorption spectra in toluene and the theoretical calculations of k_r based on the Strickler-Berg equation

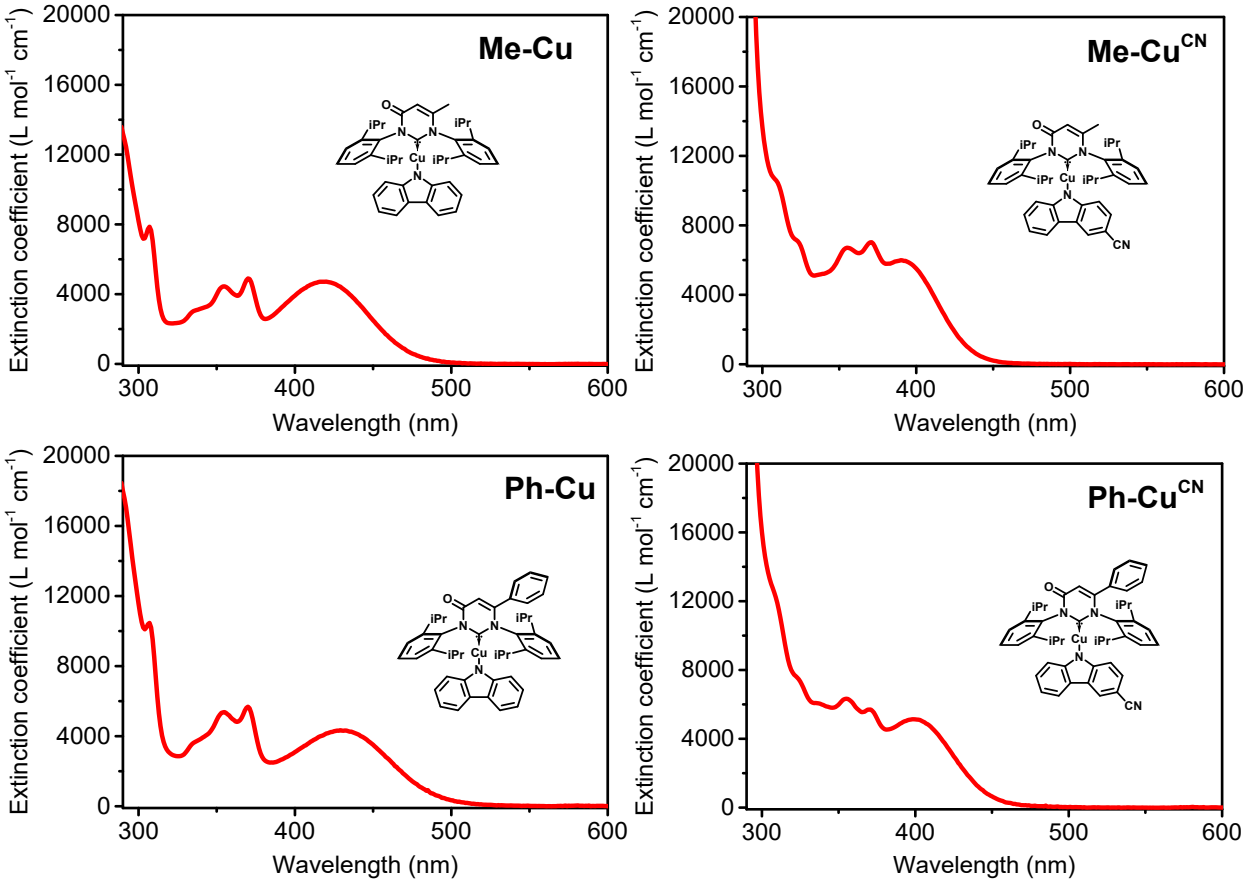

Figure S13 Absorption spectra in CH_2Cl_2 for (carbene)Cu(carbazolyl) complexes.

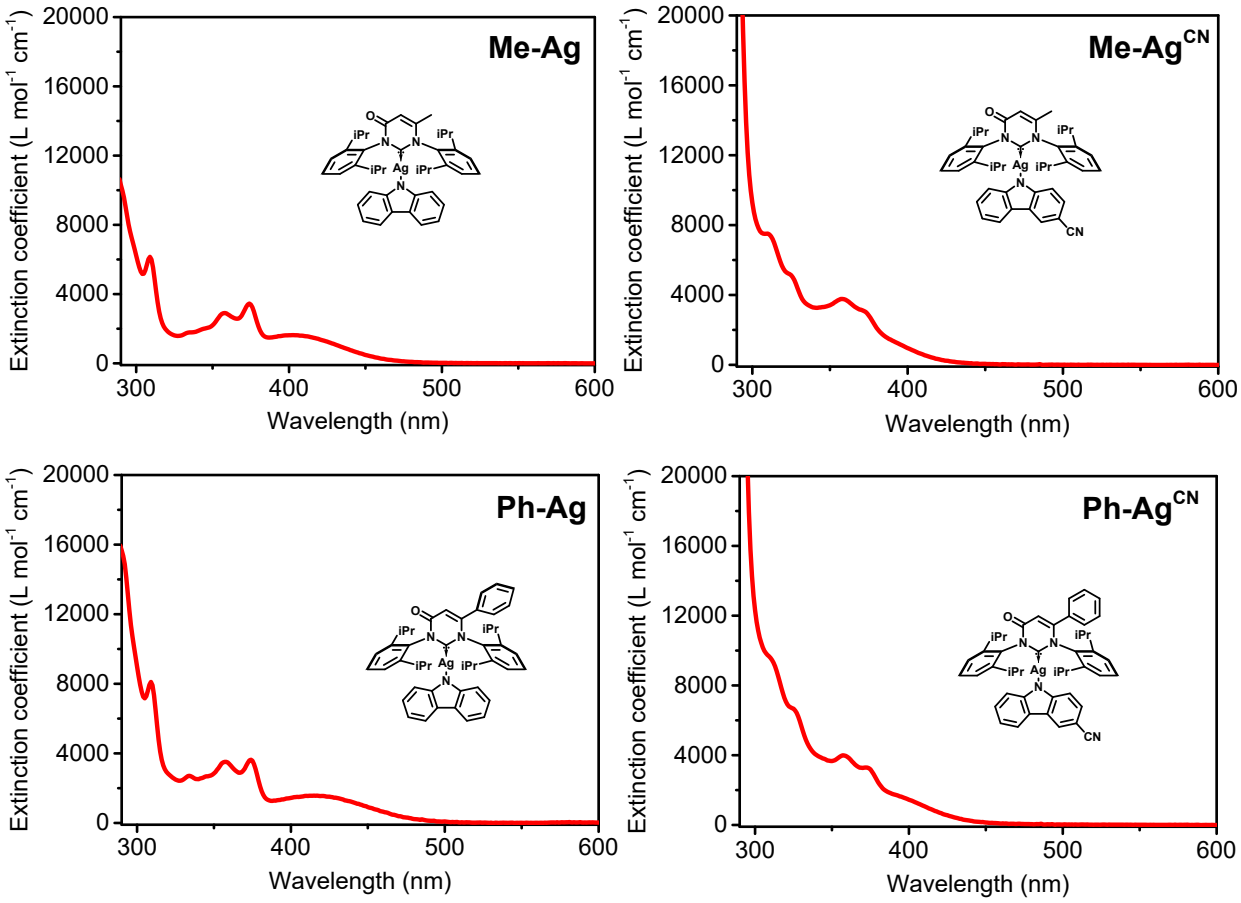

Figure S14 Absorption spectra in CH_2Cl_2 for (carbene)Ag(carbazolyl) complexes.

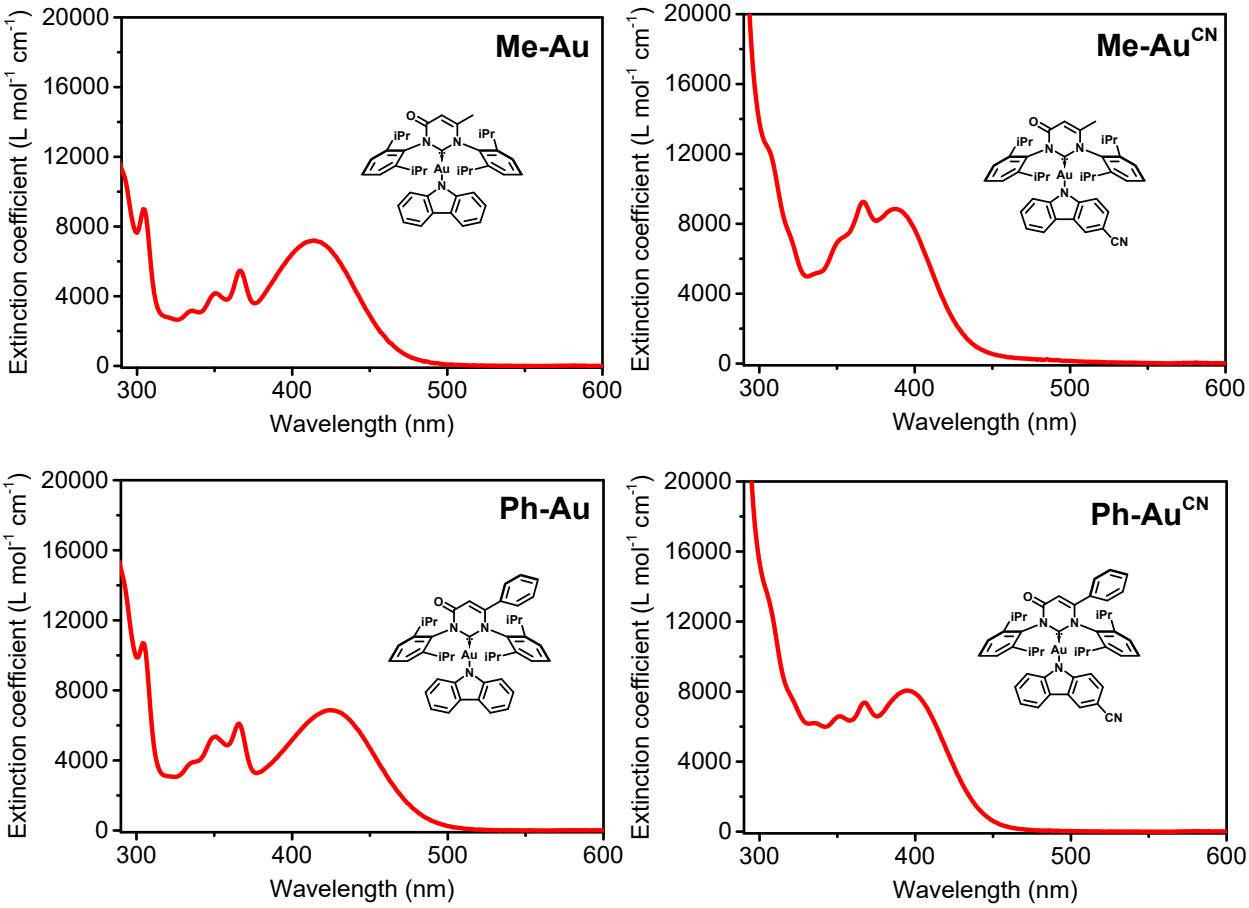

Figure S15 Absorption spectra in CH_2Cl_2 for (carbene)Au(carbazolyl) complexes.

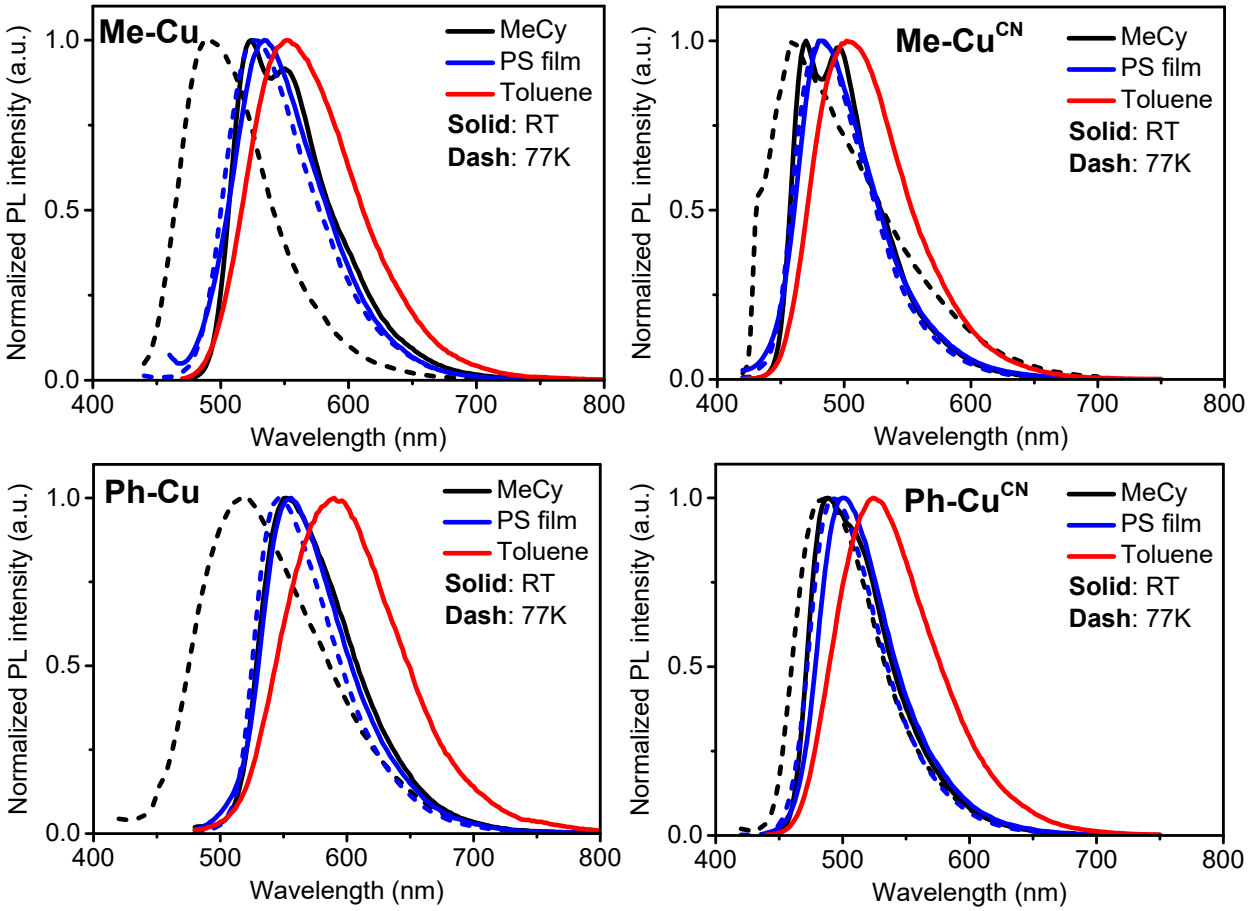

Figure S16 Emission spectra of the (carbene)Cu(carbazolyl) complexes

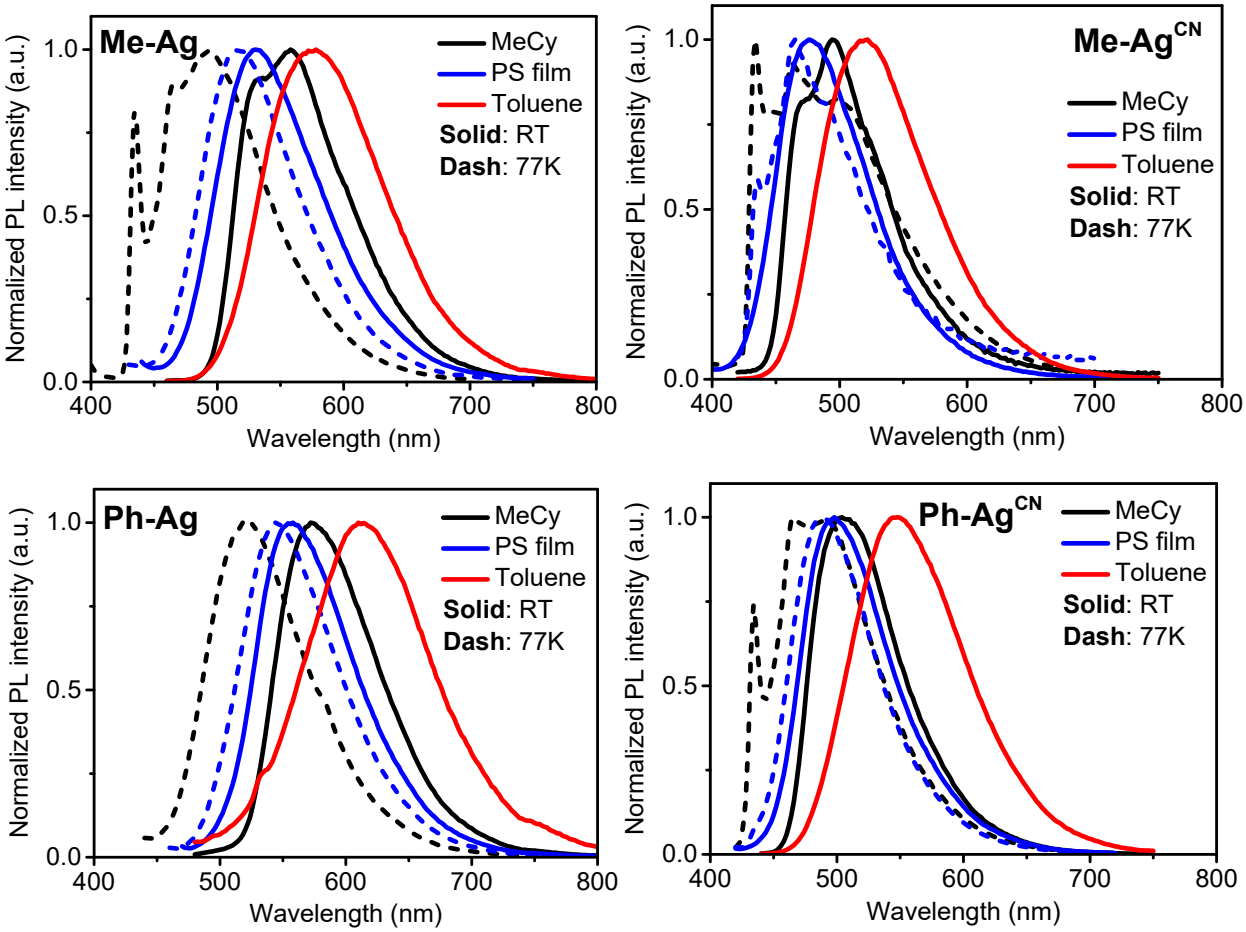

Figure S17 Emission spectra of the (carbene)Ag(carbazolyl) complexes

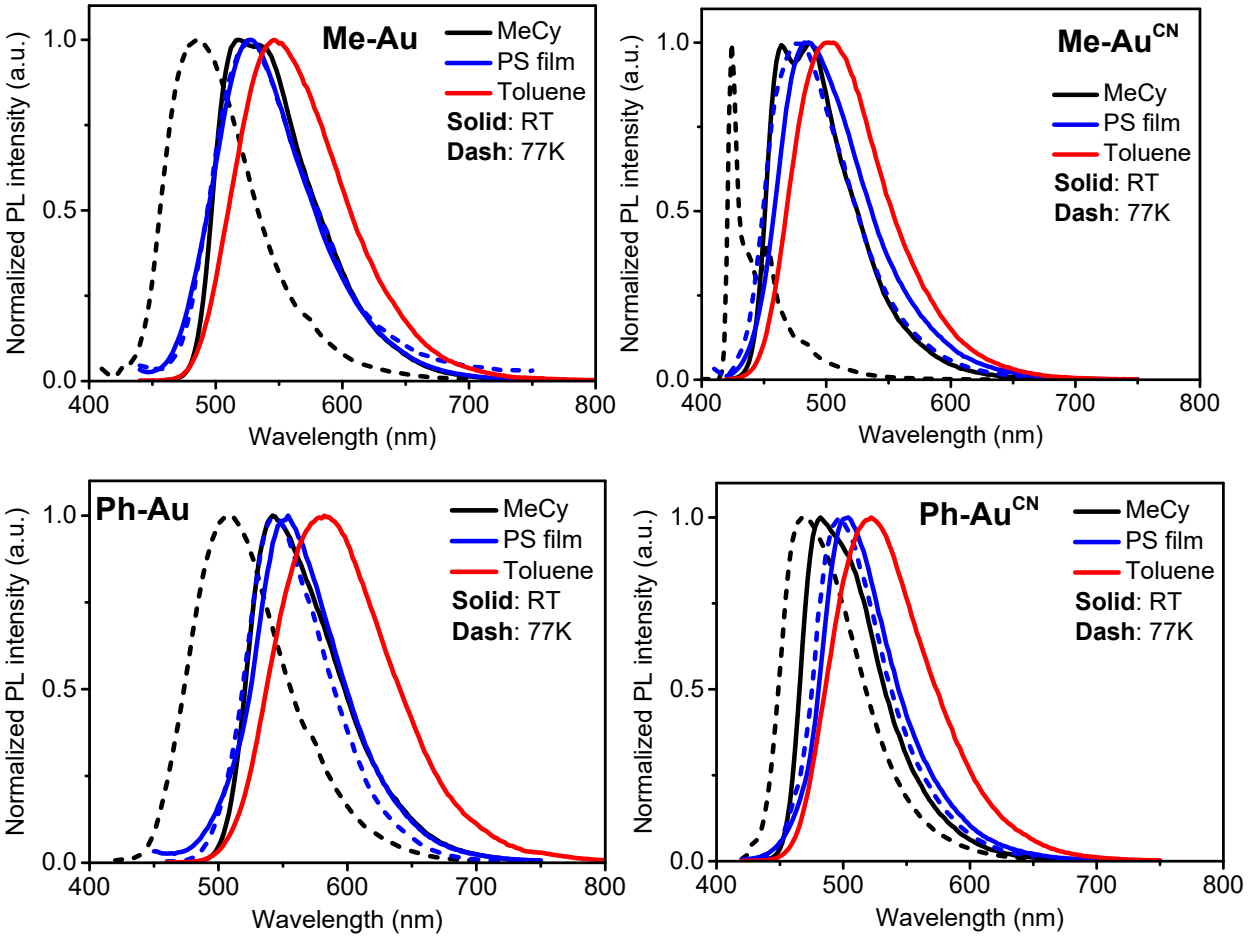

Figure S18 Emission spectra of the (carbene)Au(carbazolyl) complexes

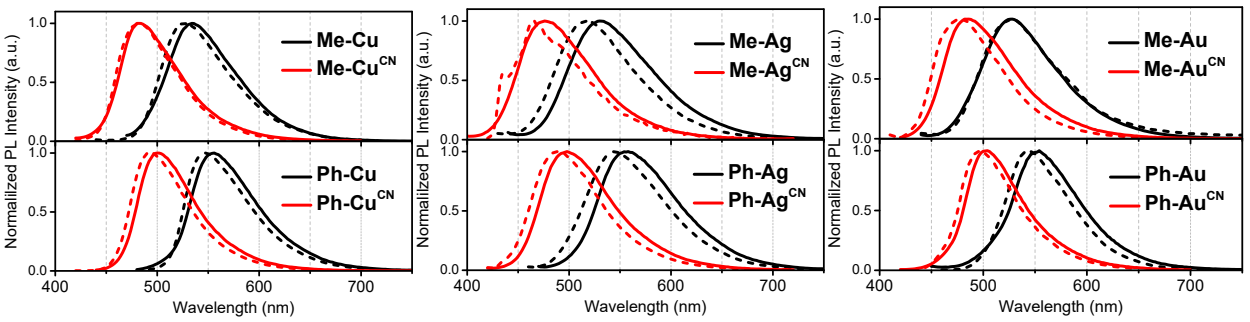

Figure S19 Emission spectra in doped PS film at room temperature (solid) and 77K (dash)

Table S7 Complete emissive photophysical properties in MeCy and 1*wt*% doped PS film

Complex	Emission at room temperature					Emission at 77K	
	λ_{max} (nm)	τ (μs)	Φ_{PL}	k_r (s^{-1})	k_{nr} (s^{-1})	λ_{max} (nm)	τ (μs)
MeCy							
Me-Cu	524, 550	1.8	0.73	4.1×10^5	1.5×10^5	490	143
Me-Cu^{CN}	470, 496	1.5	0.63	4.2×10^5	2.5×10^5	459	66
Ph-Cu	552	0.87	0.50	5.7×10^5	5.7×10^5	519	127[a]
Ph-Cu^{CN}	488	1.1	0.73	6.6×10^5	2.4×10^5	486	74
Me-Ag	533*sh*, 558	0.42	0.44	1.0×10^6	1.3×10^6	434, 493	12000[a]
Me-Ag^{CN}	470*sh*, 494	0.43	0.67	1.6×10^6	7.7×10^5	434, 463, 497	9000[a]
Ph-Ag	572	0.32	0.26	8.1×10^5	2.3×10^6	522	3.1
Ph-Ag^{CN}	504	0.61	0.55	9.0×10^5	7.4×10^5	433, 466, 490	22000[a]
Me-Au	518, 534	1.4	0.71	5.1×10^5	2.1×10^5	486	60
Me-Au^{CN}	464, 486	0.97	0.67	6.9×10^5	3.4×10^5	424, 452	328[a]
Ph-Au	542	0.80	0.60	7.5×10^5	5.0×10^5	507	85
Ph-Au^{CN}	482	0.85	0.76	8.9×10^5	2.8×10^5	469	54
1*wt*% doped PS film							
Me-Cu	534	1.5	0.58	3.9×10^5	2.8×10^5	527	265
Me-Cu^{CN}	482	1.4	0.77	5.5×10^5	1.6×10^5	482	108
Ph-Cu	556	0.97	0.70	7.2×10^5	3.1×10^5	547	93
Ph-Cu^{CN}	500	1.1	0.83	7.5×10^5	1.5×10^5	494	115
Me-Ag	530	0.41	0.77	1.9×10^6	5.6×10^5	516	7.2
Me-Ag^{CN}	476	0.41	0.83	2.0×10^6	4.1×10^5	464	6000[a]
Ph-Ag	558	0.53	0.56	1.1×10^6	8.3×10^5	544	2.7
Ph-Ag^{CN}	498	0.60	0.88	1.5×10^6	2.0×10^5	487	3.0
Me-Au	528	1.1	0.50	4.5×10^5	4.5×10^5	526	82
Me-Au^{CN}	484	0.81	0.50	6.2×10^5	6.2×10^5	478	57
Ph-Au	554	0.80	0.77	9.6×10^5	2.9×10^5	544	47
Ph-Au^{CN}	504	0.82	1.00	1.2×10^6	$<0.1\times10^5$	498	68

[a] calculated as a weighted average of the two contributions from a biexponential decay trace at emission maximum

Table S8 Φ_{PL} values of the doped PS films under air and N_2

Complex	in air	in N_2	Complex	in air	in N_2
Me-Cu	0.45	0.58	**Me-Cu^{CN}**	0.61	0.77
Ph-Cu	0.56	0.70	**Ph-Cu^{CN}**	0.70	0.83
Me-Ag	0.68	0.77	**Me-Ag^{CN}**	0.71	0.83
Ph-Ag	0.45	0.56	**Ph-Ag^{CN}**	0.77	0.88
Me-Au	0.39	0.50	**Me-Au^{CN}**	0.43	0.50
Ph-Au	0.63	0.77	**Ph-Au^{CN}**	0.88	1.00

Φ_{PL} values in N_2 were recorded when the PS film samples were fixed under N_2 stream

Table S9 Emission properties in toluene

Complex	Emission at room temperature				
	λ_{max} (nm)	τ (μs)	Φ_{PL}	k_r (s^{-1})	k_{nr} (s^{-1})
Me-Cu	552	1.5	0.66	4.4×10^5	2.3×10^5
Me-Cu^{CN}	502	1.3	0.84	6.5×10^5	1.2×10^5
Ph-Cu	590	0.17	0.10	5.9×10^5	5.3×10^6
Ph-Cu^{CN}	524	0.86	0.66	7.7×10^5	4.0×10^5
Me-Ag	578	0.18	0.23	1.3×10^6	4.3×10^6
Me-Ag^{CN}	522	0.39	0.73	1.9×10^6	6.9×10^5
Ph-Ag	610	0.038	0.02	5.3×10^5	2.6×10^7
Ph-Ag^{CN}	548	0.40	0.38	9.5×10^5	1.6×10^6
Me-Au	546	1.1	0.59	5.4×10^5	3.7×10^5
Me-Au^{CN}	502	0.87	0.71	8.2×10^5	3.3×10^5
Ph-Au	582	0.19	0.15	7.9×10^5	4.5×10^6
Ph-Au^{CN}	522	0.66	0.74	1.1×10^6	3.9×10^5

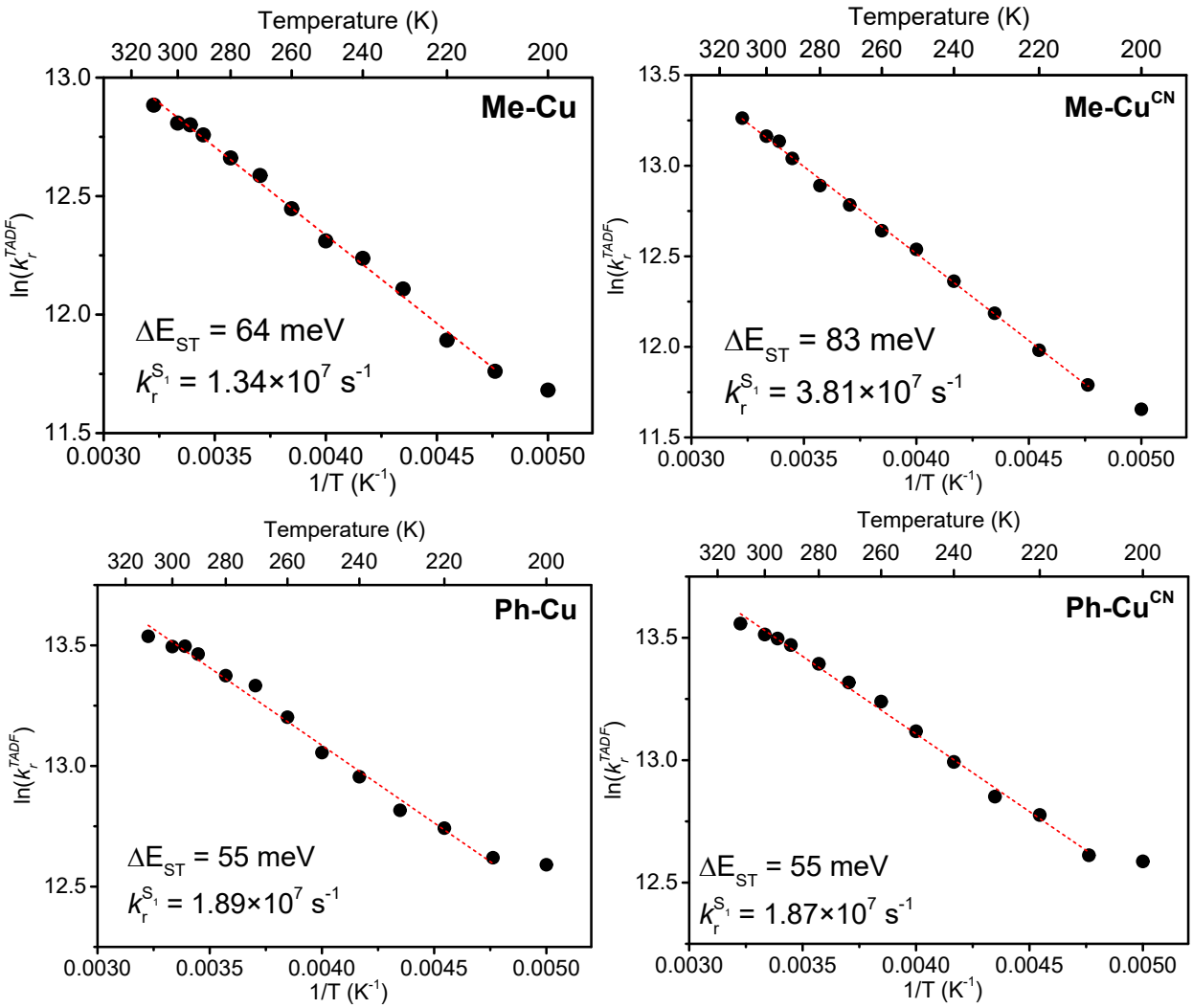

Figure S20 Full kinetic fits of the temperature dependent lifetime from 210 to 310 K for (carbene)Cu(carbazolyl) complexes.

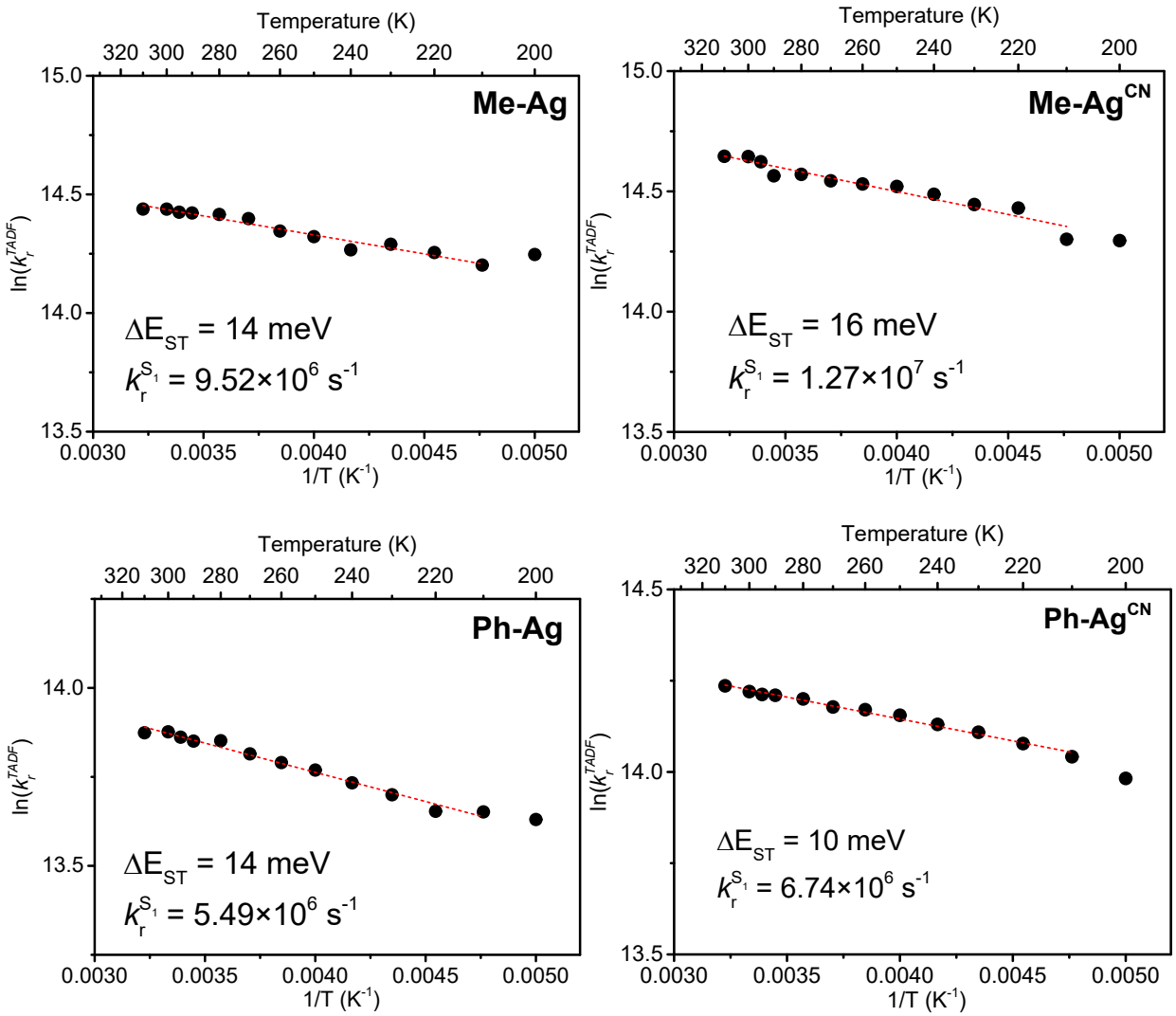

Figure S21 Full kinetic fits of the temperature dependent lifetime from 210 to 310 K for (carbene)Ag(carbazolyl) complexes.

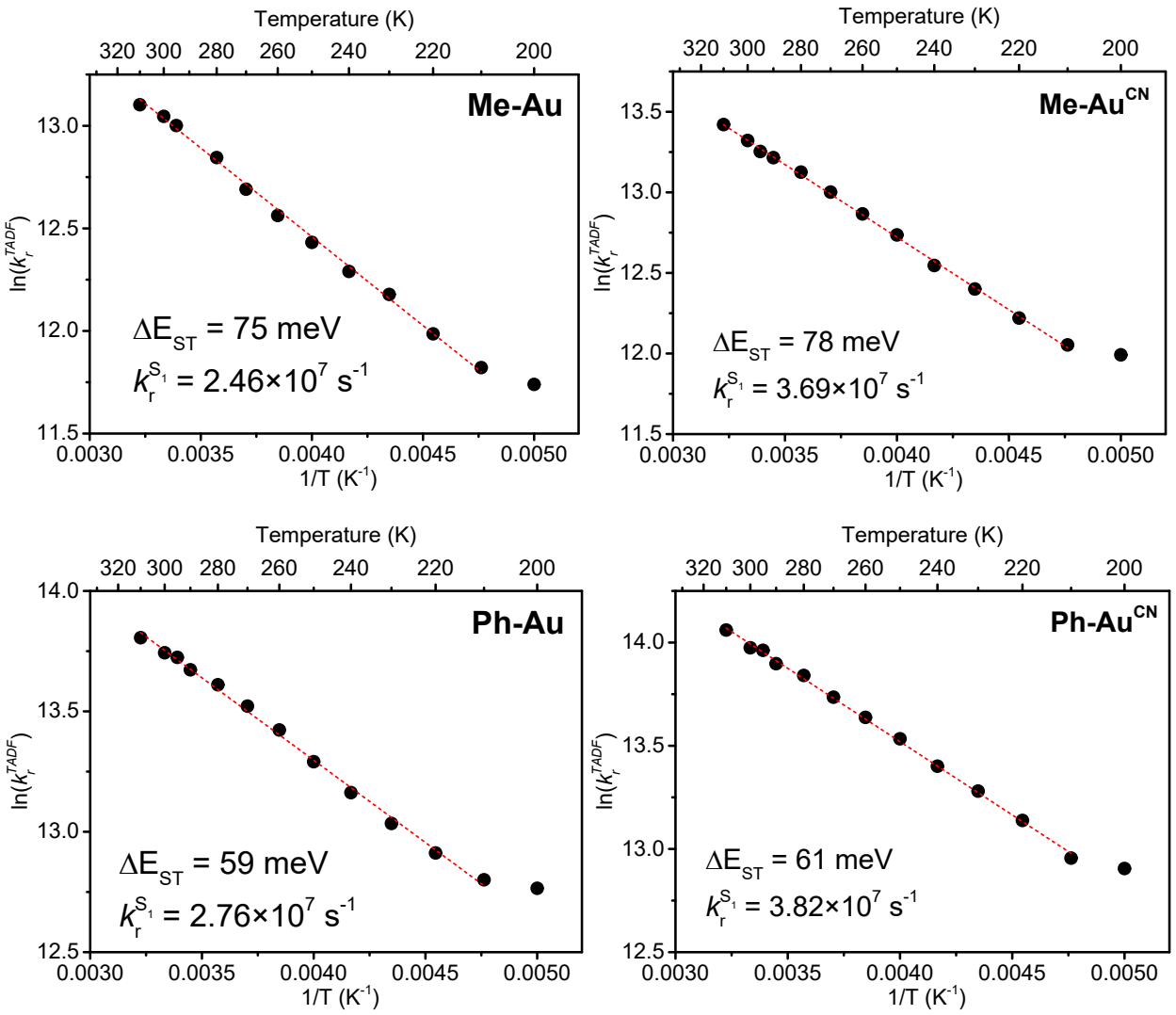

Figure S22 Full kinetic fits of the temperature dependent lifetime from 210 to 310 K for (carbene)Au(carbazolyl) complexes

Table S10 Complete photophysical properties of TADF coinage metal complexes including reported examples

Complex	NTO overlap	Φ_{PL}	τ (μs)	k_r (s^{-1})	λ_{max}^{em} (nm)	E_{em} (eV)	k_r/E^3 ($s^{-1}eV^{-3}$)	k_r^{ICT} (s^{-1})	ΔE_{ST} (meV)
Me-Cu	0.377	0.58	1.5	3.8×10^5	534	2.32	3.0×10^4	1.3×10^7	64
Me-Cu^{CN}	0.361	0.77	1.4	5.4×10^5	480	2.58	3.1×10^4	3.8×10^7	83
Ph-Cu	0.311	0.70	0.98	7.2×10^5	556	2.23	6.5×10^4	1.9×10^7	55
Ph-Cu^{CN}	0.301	0.83	1.1	7.3×10^5	500	2.48	4.8×10^4	1.9×10^7	55
(CAAC)CuCz[3]	0.379	-	-	3.5×10^5	474	2.62	1.9×10^4	1.4×10^7	73
(MAC)CuCz[4]	0.366	-	-	6.4×10^5	506	2.45	4.3×10^4	3.6×10^7	71
Me-Ag	0.268	0.77	0.41	1.9×10^6	530	2.34	1.5×10^5	9.5×10^6	14
Me-Ag^{CN}	0.272	0.83	0.41	2.0×10^6	476	2.60	1.1×10^5	1.3×10^7	16
Ph-Ag	0.212	0.56	0.53	1.1×10^6	558	2.22	9.6×10^4	5.5×10^6	14
Ph-Ag^{CN}	0.211	0.88	0.60	1.5×10^6	498	2.49	9.5×10^4	6.7×10^6	10
(CAAC)AgCz[5]	0.288	-	-	2.0×10^6	472	2.63	1.1×10^5	1.2×10^7	19
(MAC)AgCz[5]	0.280	-	-	2.4×10^6	512	2.42	1.7×10^5	2.2×10^7	22
Me-Au	0.411	0.50	1.1	4.7×10^5	528	2.35	3.6×10^4	2.5×10^7	75
Me-Au^{CN}	0.391	0.50	0.81	6.1×10^5	484	2.56	3.6×10^4	3.7×10^7	78
Ph-Au	0.342	0.77	0.79	9.6×10^5	554	2.24	8.6×10^4	2.8×10^7	59
Ph-Au^{CN}	0.364	1.0	0.82	1.2×10^6	504	2.46	8.2×10^4	3.8×10^7	61
(CAAC)AuCz[5]	0.418	-	-	8.8×10^5	472	2.63	4.9×10^4	4.0×10^7	71
(MAC)AuCz[5]	0.400	-	-	1.0×10^6	512	2.42	7.0×10^4	4.2×10^7	71
Au-1c[8]	0.333	-	-	5.8×10^5	620	2.00	7.3×10^4	6.7×10^7	100
Au-2d[8]	0.373	-	-	2.2×10^5	504	2.46	1.5×10^4	4.2×10^7	119
Au-2d-Me[8]	0.381	-	-	1.9×10^5	520	2.38	1.4×10^4	3.0×10^7	105
Au-2e[8]	0.367	-	-	2.4×10^5	544	2.28	2.0×10^4	4.0×10^7	109
Au-2e-Me[8]	0.373	-	-	2.0×10^5	554	2.24	1.8×10^4	4.0×10^7	113
Au^{CC6}	0.289	-	-	1.5×10^6	480	2.58	8.7×10^4	3.1×10^7	50

The relative PLQY Φ_{PL} at different temperature is calculated according to the following equation

$$\Phi_{PL} = \frac{A}{A_{295K}} \times \Phi_{PL,295K}$$

where A and A_{295K} are the integrated emission spectra area at the corresponding temperature and 295K, respectively. $\Phi_{PL,295K}$ is the absolute PLQY at 295K.

Table S11 Relative Φ_{PL} in doped PS film at different temperature

Temperature (K)	**Me-Cu**	**Me-Cu^{CN}**	**Ph-Cu**	**Ph-Cu^{CN}**
210	0.69	0.68	0.72	0.89
220	0.68	0.69	0.72	0.88
230	0.66	0.70	0.72	0.87
240	0.65	0.72	0.72	0.88
250	0.63	0.73	0.72	0.88
260	0.62	0.74	0.73	0.8
270	0.61	0.75	0.73	0.88
280	0.60	0.74	0.73	0.86
290	0.58	0.76	0.74	0.84
300	0.57	0.77	0.70	0.82
310	0.55	0.77	0.69	0.81
Temperature (K)	**Me-Ag**	**Me-Ag^{CN}**	**Ph-Ag**	**Ph-Ag^{CN}**
210	0.94	0.88	0.59	0.92
220	0.92	0.86	0.58	0.92
230	0.90	0.85	0.58	0.91
240	0.85	0.85	0.58	0.91
250	0.84	0.84	0.58	0.92
260	0.82	0.83	0.58	0.91
270	0.81	0.83	0.57	0.90
280	0.80	0.82	0.57	0.89
290	0.78	0.81	0.57	0.88
300	0.76	0.84	0.55	0.88
310	0.74	0.83	0.55	0.86
Temperature (K)	**Me-Au**	**Me-Au^{CN}**	**Ph-Au**	**Ph-Au^{CN}**
210	0.54	0.78	0.75	1.0
220	0.54	0.48	0.75	1.0
230	0.54	0.49	0.76	1.0
240	0.53	0.50	0.76	1.0
250	0.53	0.50	0.77	1.0
260	0.52	0.50	0.77	1.0
270	0.52	0.50	0.77	1.0
280	0.51	0.50	0.77	1.0
290	0.51	0.50	0.77	1.0
300	0.50	0.50	0.76	1.0
310	0.49	0.50	0.75	1.0

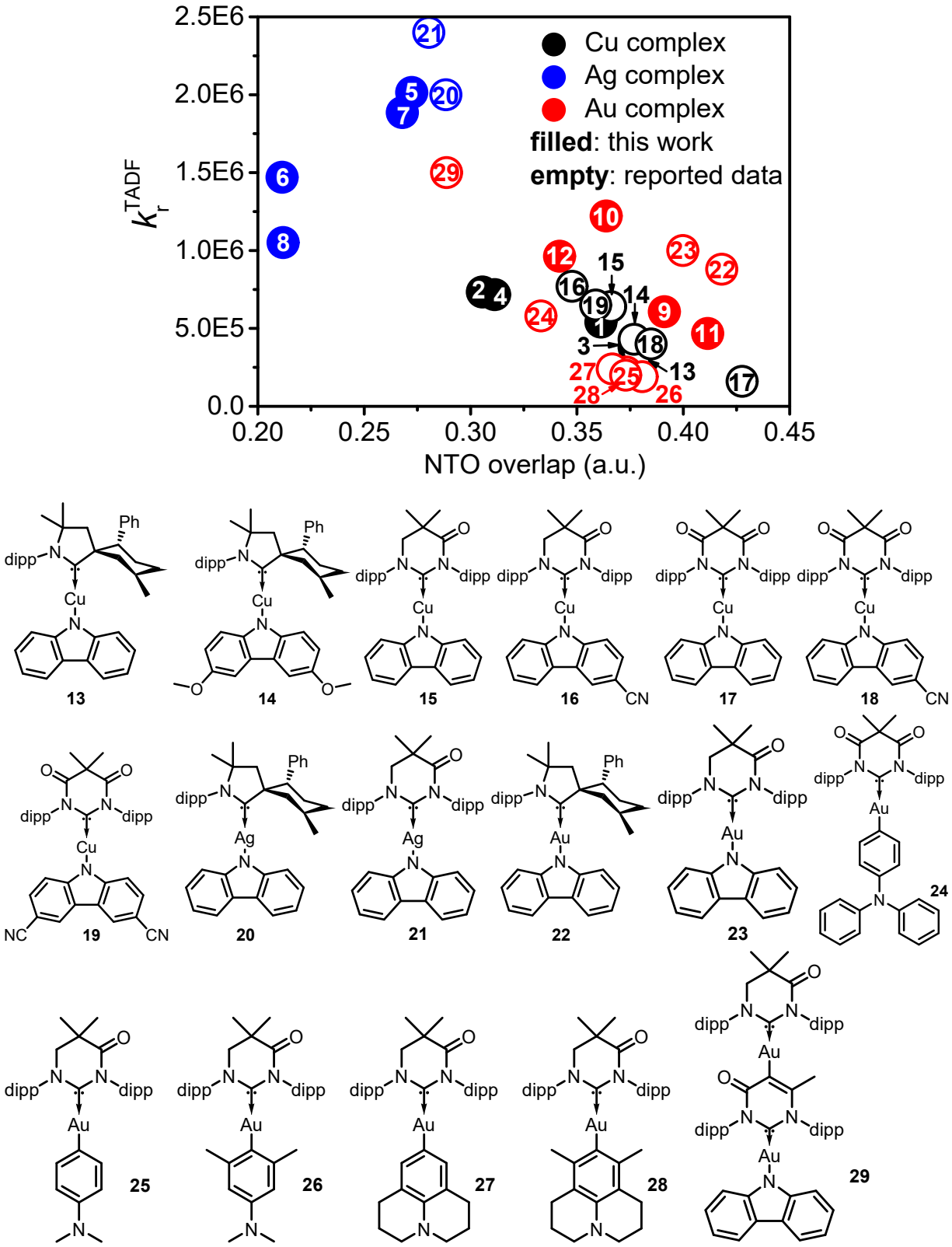

Figure S23 TADF radiative decay rate as a function of NTO overlap with structures of reported molecules

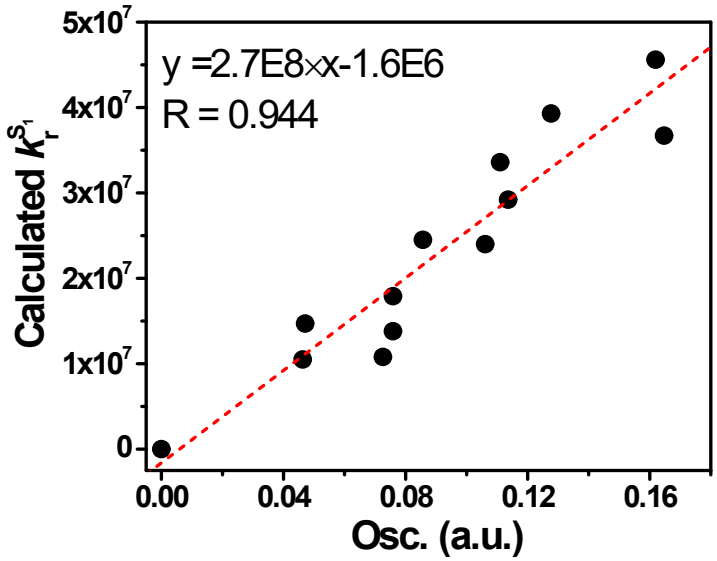

Figure S24 Relationship between calculated $k_r^{S_1}$ by Strickler-Berg equation and Osc. Strength based on the new coinage metal complexes

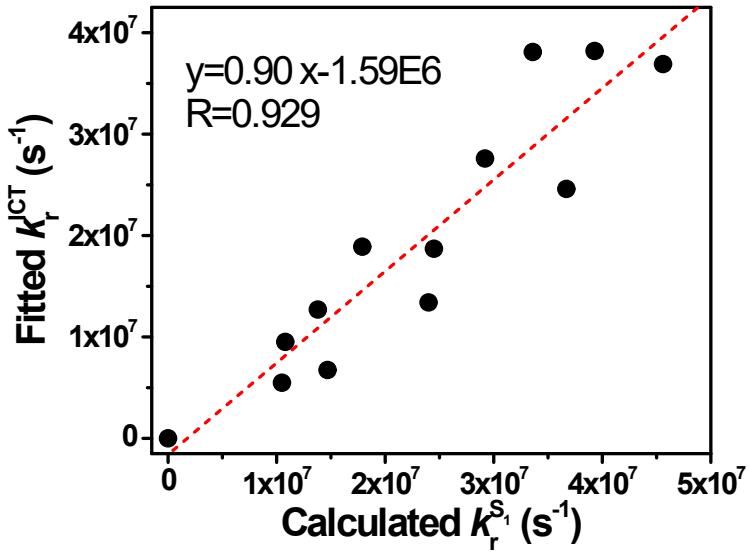

Figure S25 Relationship between the experimentally fitted $k_r^{S_1}$ and calculated $k_r^{S_1}$ by Strickler-Berg equation

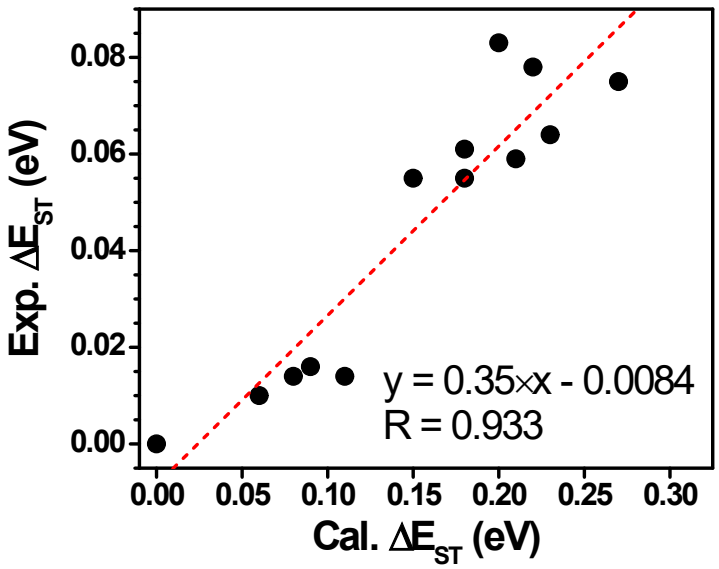

Figure S26 Relationship between experimental and theoretically calculated ΔE_{ST}

Table S12 Photophysical properties of some reported highly efficient organic TADF molecules

Acronym	Molecular structure	NTO over lap	ΔE_{ST} (Exp.)	ΔE_{ST} (Cal.)	k_r(S1) (s^{-1})	ISC rate (s^{-1})	k_r(TADF) (s^{-1})	Ref.
4CzIPN	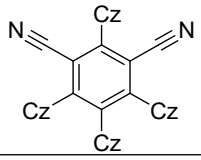	0.3802	0.04 eV in toluene	0.25 eV	1.8E7	k_{ISC} 7.0E7 k_{RISC} 8.8E5	1.41E5	9
5CzBN	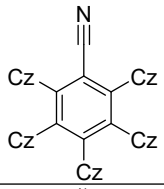	0.3336	0.17eV in toluene	0.17 eV	1.9E7	k_{ISC} 25E7 k_{RISC} 2.2E5	1.45E4	9
3Cz2DPhCzBN	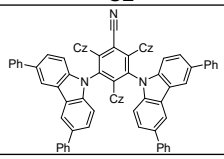	0.3900	0.15eV in toluene	0.37 eV	1.5E7	k_{ISC} 15E7 k_{RISC} 7.2E5	5.90E4	10
5Cz-TRZ	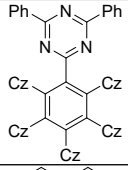	0.2956	0.06eV in toluene	0.31 eV	0.544E7	k_{ISC} 17E7 k_{RISC} 1.5E7	4.84E5	11
n-DABNA	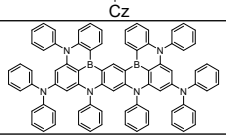	0.5864	0.017eV in toluene	0.45 eV	20E7	k_{ISC} 2.3E7 k_{RISC} 2.0E5	1.95E4	12

TMCz-BO	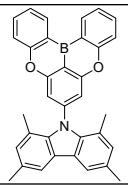	0.22 36	0.020eV in 30% doped PPF	0.21 eV	1.7E7	k_{ISC} 0.9E7 k_{RISC} 19E5	4.27E5	13
Br-3-PXZ-XO	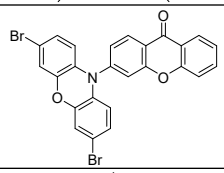	0.18 36	N/A	0.09 eV	0.68E7	k_{ISC} 19E7 k_{RISC} 260E5	8.57E5	14
DiKTa	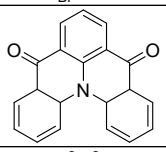	0.58 52	0.20eV in 3.5% doped mCP	0.79 eV	4.9E7	k_{ISC} 0.75E7 k_{RISC} 0.46E5	1.13E4	15
DMAC-DPS	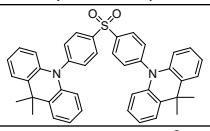	0.20 06	0.08eV in toluene	0.05 eV	On the order of E7	k_{ISC} 3.7E7	9.01E4	16
MXAc-CM	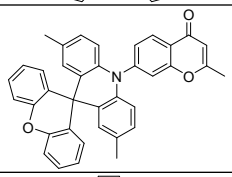	0.18 60	0.08eV in 25% doped PPF film	0.06 eV	1.1E7	k_{ISC} 2.0E7 k_{RISC} 6.7E5	1.52E5	17
AmT	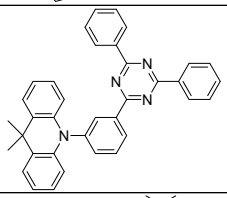	0.17 04	0.034 eV In neat film	0.03 eV	1.7E6	k_{ISC} 3.3E6 k_{RISC} 1.3E6	8.33E4	18
MPAc-BS	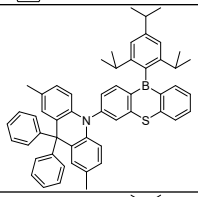	0.23 55	0.023eV 50% doped PPF host matrix	0.54 eV	2.8E7	k_{ISC} 9.9E7 k_{RISC} 3.5E6	6E5	19
MPAc-BO	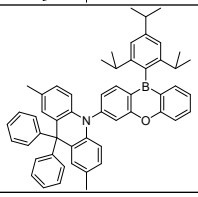	0.26 33	0.024eV 50% doped PPF host matrix	0.68 eV	1.9E7	k_{ISC} 1.7E7 k_{RISC} 1.0E6	2.61E5	19
TPA-DCPP	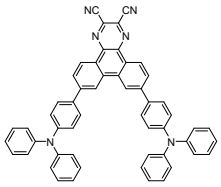	0.52 81	0.13eV In toluene By emission onset differenc es	0.64 eV	10.7E7	N/A	N/A	20
BCzT	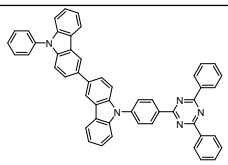	0.50 34	0.31eV In doped DPEPO film By emission	0.60 eV	18.2E7	k_{ISC}=2.7E7 k_{RISC}=4.0E3	4.27E3	21

			onset differences					
Ph3Cz-TRZ	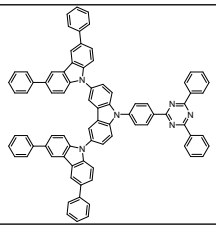	0.4205	0.11eV In 6 wt% doped DPEPO film	0.61 eV	1.6E7	k_{ISC}=2.9E7	N/A	22
DABNA-1	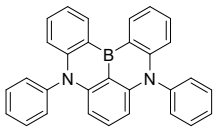	0.5970	0.20eV In 1% doped mCBP film	0.57 eV	11.4E7	k_{ISC} =4.5E6 k_{RISC} =9.9E3	3.74E2	23
SpiroAc-TRZ	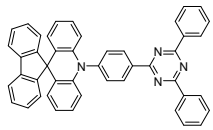	0.1594	0.072 12% doped mCPCN film	0.04 eV	5.9E7	k_{ISC} =9.8E6 k_{RISC}=1.26E5	1.00E5	24
DMAC-BP	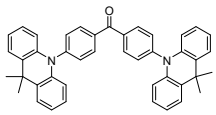	0.2065	0.07 In 10% doped mCP film	0.20 eV	N/A	N/A	N/A	25
DBT-BZ-DMAC	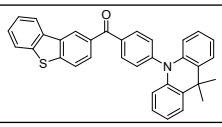	0.1807	0.08eV in neat film	0.24 eV	2.5E7	k_{ISC} =1.6E7 k_{RISC} =4.6E5	2.75E5	26
ACRDSO2	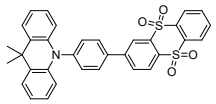	0.1353	0.058eV In 6% doped CBP	0.008 eV	2.4E7	k_{ISC} =5.11E6 k_{RISC} =9.6E4	4.94E4	27
PXZDSO2	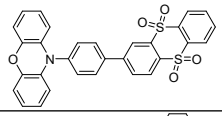	0.1599	0.048eV In 6% doped CBP	0.018 eV	2.8E7	k_{ISC} =6.2E6 k_{RISC} =4.6E4	5.80E4	27
PXZ-TRZ	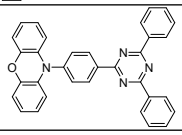	0.1608	0.08eV In 6% doped CBP film	0.012 eV	5E7	N/A	N/A	28

References

1. J. Wang, X. Cao, S. Lv, C. Zhang, S. Xu, M. Shi and J. Zhang, *Nat. Commun.*, 2017, **8**, 14625.
2. C. Zhang, F. Zhang, S. Lv, M. Shi and J. Zhang, *New J. Chem.*, 2017, **41**, 1889-1892.
3. R. Hamze, J. L. Peltier, D. Sylvinson, M. Jung, J. Cardenas, R. Haiges, M. Soleilhavoup, R. Jazzar, P. I. Djurovich, G. Bertrand and M. E. Thompson, *Science*, 2019, **363**, 601.
4. S. Shi, M. C. Jung, C. Coburn, A. Tadle, D. Sylvinson M. R, P. I. Djurovich, S. R. Forrest and M. E. Thompson, *J. Am. Chem. Soc.*, 2019, **141**, 3576-3588.
5. R. Hamze, S. Shi, S. C. Kapper, D. S. Muthiah Ravinson, L. Estergreen, M.-C. Jung, A. C. Tadle, R. Haiges, P. I. Djurovich, J. L. Peltier, R. Jazzar, G. Bertrand, S. E. Bradforth and M. E. Thompson, *J. Am. Chem. Soc.*, 2019, **141**, 8616-8626.
6. T.-y. Li, D. G. Shlian, P. I. Djurovich and M. E. Thompson, *Chem. Eur. J.*, 2021, **27**, 6191-6197.
7. A. C. Tadle, K. A. El Roz, C. H. Soh, D. Sylvinson Muthiah Ravinson, P. I. Djurovich, S. R. Forrest and M. E. Thompson, *Adv. Funct. Mater.*, 2021, **31**, 2101175.
8. T.-y. Li, D. S. Muthiah Ravinson, R. Haiges, P. I. Djurovich and M. E. Thompson, *J. Am. Chem. Soc.*, 2020, **142**, 6158-6172.
9. H. Noda, X.-K. Chen, H. Nakanotani, T. Hosokai, M. Miyajima, N. Notsuka, Y. Kashima, J.-L. Brédas and C. Adachi, *Nat. Mater.*, 2019, **18**, 1084-1090.
10. H. Noda, H. Nakanotani and C. Adachi, *Sci. Adv.*, 2018, **4**, 6910.
11. L.-S. Cui, A. J. Gillett, S.-F. Zhang, H. Ye, Y. Liu, X.-K. Chen, Z.-S. Lin, E. W. Evans, W. K. Myers, T. K. Ronson, H. Nakanotani, S. Reineke, J.-L. Bredas, C. Adachi and R. H. Friend, *Nat. Photonics*, 2020, **14**, 636-642.
12. Y. Kondo, K. Yoshiura, S. Kitera, H. Nishi, S. Oda, H. Gotoh, Y. Sasada, M. Yanai and T. Hatakeyama, *Nat. Photonics*, 2019, **13**, 678-682.
13. J. U. Kim, I. S. Park, C.-Y. Chan, M. Tanaka, Y. Tsuchiya, H. Nakanotani and C. Adachi, *Nat. Commun.*, 2020, **11**, 1765.
14. N. Aizawa, Y. Harabuchi, S. Maeda and Y.-J. Pu, *Nat. Commun.*, 2020, **11**, 3909.
15. D. Hall, S. M. Suresh, P. L. dos Santos, E. Duda, S. Bagnich, A. Pershin, P. Rajamalli, D. B. Cordes, A. M. Z. Slawin, D. Beljonne, A. Köhler, I. D. W. Samuel, Y. Olivier and E. Zysman-Colman, *Adv. Opt. Mater.*, 2020, **8**, 1901627.
16. Q. Zhang, B. Li, S. Huang, H. Nomura, H. Tanaka and C. Adachi, *Nat. Photonics*, 2014, **8**, 326-332.
17. J. Lee, N. Aizawa and T. Yasuda, *Chem. Mater.*, 2017, **29**, 8012-8020.
18. S. Jeong, Y. Lee, J. K. Kim, D.-J. Jang and J.-I. Hong, *J. Mater. Chem. C*, 2018, **6**, 9049-9054.
19. I. S. Park, K. Matsuo, N. Aizawa and T. Yasuda, *Adv. Funct. Mater.*, 2018, **28**, 1802031.
20. S. Wang, X. Yan, Z. Cheng, H. Zhang, Y. Liu and Y. Wang, *Angew. Chem. Int. Ed.*, 2015, **54**, 13068-13072.
21. K. Shizu, H. Noda, H. Tanaka, M. Taneda, M. Uejima, T. Sato, K. Tanaka, H. Kaji and C. Adachi, *The Journal of Physical Chemistry C*, 2015, **119**, 26283-26289.
22. S. Hirata, Y. Sakai, K. Masui, H. Tanaka, S. Y. Lee, H. Nomura, N. Nakamura, M. Yasumatsu, H. Nakanotani, Q. Zhang, K. Shizu, H. Miyazaki and C. Adachi, *Nat. Mater.*, 2015, **14**, 330-336.
23. T. Hatakeyama, K. Shiren, K. Nakajima, S. Nomura, S. Nakatsuka, K. Kinoshita, J. Ni, Y. Ono and T. Ikuta, *Adv. Mater.*, 2016, **28**, 2777-2781.
24. T.-A. Lin, T. Chatterjee, W.-L. Tsai, W.-K. Lee, M.-J. Wu, M. Jiao, K.-C. Pan, C.-L. Yi, C.-L. Chung, K.-T. Wong and C.-C. Wu, *Adv. Mater.*, 2016, **28**, 6976-6983.
25. Q. Zhang, D. Tsang, H. Kuwabara, Y. Hatae, B. Li, T. Takahashi, S. Y. Lee, T. Yasuda and C. Adachi, *Adv. Mater.*, 2015, **27**, 2096-2100.
26. J. Guo, X.-L. Li, H. Nie, W. Luo, S. Gan, S. Hu, R. Hu, A. Qin, Z. Zhao, S.-J. Su and B. Z. Tang, *Adv. Funct. Mater.*, 2017, **27**, 1606458.
27. G. Xie, X. Li, D. Chen, Z. Wang, X. Cai, D. Chen, Y. Li, K. Liu, Y. Cao and S.-J. Su, *Adv. Mater.*, 2016, **28**, 181-187.
28. H. Tanaka, K. Shizu, H. Miyazaki and C. Adachi, *Chem. Commun.*, 2012, **48**, 11392-11394.